TRANSFORMATION OPTICS BASED FINITE-DIFFERENCE
TIME-DOMAIN SIMULATION
OF SUPERSCATTERING

by

ANDRE' J STRONG

A DISSERTATION

Submitted in partial fulfillment of the requirements for the degree of
Doctor of Philosophy in the Interdisciplinary Applied Mathematics and
Mathematical Physics Doctoral Program of
Delaware State University

DOVER, DELAWARE
December 2018

This dissertation is approved by the following members of the Final Oral Review Committee:

Dr. Jinjie Liu, Committee Chairperson, Division of Physical and Computational Sciences, Delaware State University
Dr. Moysey Brio, External Committee Member, Department of Mathematics, University of Arizona
Dr. Aristides Marcano, Committee Member, Division of Physical and Computational Sciences, Delaware State University
Dr. Essaid Zerrad, Committee Member, Division of Physical and Computational Sciences, Delaware State University
Dr. Matthew Tanzy, Committee Member, Division of Physical and Computational Sciences, Delaware State University

DEDICATION

I would like to first dedicate this dissertation to my grandmother Mrs. Bettie Davis strong. She was a strong God fearing woman. She was a very hardworking woman and a very great cook. She had her own catering service and was the best cook and caterer in Memphis Tennessee. She catered a party for Minister Farakan which consisted of twenty-five hundred guests. She also catered a party for the legendary Bo Jackson. My grandmother was very famous for her monkey bread. She was always in the kitchen making a loaf for either her church, a guest, or her family. Each Christmas she would host a brunch for her grandchildren only where she would make her famous monkey bread and cheese grits. My grandmother taught me how to cook, wash clothes, and wash dishes. My nickname to her was ”Love”. Every morning I would call her and say, ”Hey Love, how you be?”. I really loved talking on the phone with my grandmother and watching TV with her. She will truly be missed.

I next want to dedicate this dissertation to my uncle Alvin Strong Sr. My uncle Alvin showed me a lot about being a man. He would tell me things like stand up straight with your chest out, always look a person in the eyes when you're speaking to them, always have a firm hand shake, speak up, and speak clearly when you're talking to someone. My mom would always take him on road trips with her to different cities. He loved to swim, play basketball with his kids, and plant in his garden. He was also a great cook just like his mother, my grandmother. My grandmother would always take him to parties she had to cater and sometimes he would even be the bartender. He served his country in the Army and was honorably discharged due to an injury to his eye. He became legally blind in his right eye as a result of an injury he sustained in the Army. He will truly be missed.

I also would like to dedicate this dissertation to my mother, Rev. Dr. Terri Strong. My mom has been a true inspiration to me my entire life. A single parent raising a young black man is a very difficult task. I watched my mom go to work everyday. She made sure that I never went without and she would always buy me whatever I wanted for Christmas. When I was in the sixth grade I received an unsatisfactory grade in pre-algebra and my mom gave me a very firm chastising for it. It has always been implied that this particular chastising is what triggered my excellence in mathematics, so as a result I received three degrees in mathematics. Thank you mom for that stern chastising. My mom is the youngest child of ten siblings and she is the only one that has a college degree. My mom has an associates in Applied Science, she has a bachelors in Business Administration, a masters in Divinity, and a Doctorate in Ministry. She's an ordained Itinerant Elder of the African Methodist Episcopal Church and she's on the ministerial staff at our home church. She worked as a supervisor for the Sheriff's office for twenty-five years and she is now retired. She actually just received her doctorate in ministry this year, May 12, 2018, so my mom and I both received our doctorate degrees in the same year. I love you mom and may God continue to bless you.

I next would like to recognize my ninth grade algebra teacher Mr. Cedric Shannon. Mr. Shannon brought out a talent in me I never knew I had. I was his smartest algebra student in class. He told me, "Son when you go to college, major in mathematics". When I entered college and an advisor asked me what I would like to major in, all I could hear was him saying, "Son, when you go to college, major in mathematics", and so as a result that's what I did. Back in 2010 I found him on Facebook. He stated to me that he has seen where I graduated from college and wanted to know what I earned a degree in, I in turned told him, "Well you told me to major in mathematics when I went to college, so that's what I got my degree in". That was like a breath of fresh air being able to tell him that. Now I have received a PhD in it. To God be the glory. Thank you Mr. Shannon.

Last but certainly not least I would like to dedicate this dissertation to my professor back in Tennessee Dr. Sathananthan. That man believed in me. He saw a future for me that I didn't see for myself. He is the one that insisted that I pursue the PhD in mathematics.

Doing research for him was nothing short of amazing. He always made sure that I was under a grant making a good salary. He took me to different international conferences where I would give talks about my research. He helped me to acquire two publications during my graduate studies, and he made sure that I got accepted to a PhD program. Dr. Sathananthan is a very just man and he treats his students almost better than he treats his own children. Thank you for your training Dr. Sathananthan. You are truly a man of honor.

ACKNOWLEDGEMENTS

I would like to express my deepest, sincerest, and earnest appreciation and gratitude to my dissertation advisor Dr. Jinjie Liu. I want to thank you for giving me the opportunity to work under you, for exercising great patience with me, and making sure that I completed the program. You made sure that I understood every concept of this research. Your training can not be matched Dr. Jinjie Liu. The assistance you provided throughout my studies was phenomenal. You are a very diligent worker. I am forever indebted to you Doc! Thank you for the ICERM conference trip. It was very helpful and exciting. I really enjoyed Providence Rhode Island. What a beautiful city. The conference was nothing short of amazing. The people were very welcoming. Dr. Jinjie Liu, you are nothing short of an amazing kind hearted person. You are also a very witty guy. You have a wonderful sense of humor. I am looking forward to doing research with you in the near future. I would love to be a collaborator of yours.

Next I would like to acknowledge Dr. Dawn Lott for diligently helping me throughout this program. I thank you for your warm words of encouragement, the sound advice that you continued to share with me, and the wisdom you bestowed upon me. You are indeed a very true friend. Your reputation precedes you. I do not want this friendship to end. I hope in the near future that we can collaborate on a number of projects. I will seek wise counsel from you throughout my tenure. You are a woman of great knowledge and wisdom. You also give back to the community. Continue being a beacon of light for Christ. Thank you for being a friend.

To Jacquelyn Jones, without you I would be broke and hungry. You are the most effective administrator I have ever encountered in my studies. You work nonstop around the clock and you are always ten steps ahead. You work cannot be matched. You are a very warm

hearted person. You really go the extra mile for your students. For that I say thank you Jackie. I really look forward to working with you in the near future in whatever endeavors you may embark upon. You were a listening ear and a shoulder to cry on. I pray The Lord continues to shower down blessings upon you.

ABSTRACT

In this dissertation we study the Transformation Optics Finite Difference Time-Domain (TO-FDTD) method. We show how applying a coordinate transformation can be employed to map an irregular mesh to a cartesian mesh. We apply the anisotropic FDTD method to solve the transformed Maxwell's equation in the new transformed grid. To validate our claim we model the local field near the metallic nanoparticles and superscattering. The TO method achieves the same level of accuracy or more with half the grid size mesh as the standard FDTD, and the computational cost is reduced compared to the standard FDTD method.

TABLE OF CONTENTS

LIST OF TABLES

LIST OF FIGURES OR ILLUSTRATION

Chapter 1

INTRODUCTION

1.1 Introduction

In this work we study the well known Maxwell's Equations for electrodynamics. These equations were published in 1861 by a Scottish physicist and mathematician by the name of James Clerk Maxwell. These equations are composed of an electric field and a magnetic field, thus they show the existence of electromagnetic waves propagating through vacuum and matter. The equations are known as Gauss's Law, Guass's Law for Magnetism, Faraday's Law of Induction, and Ampere's Law. To solve the Maxwell's equations Kane Yee developed an algorithm in 1966, which employs second-order central differences that approximates both spatial and time derivatives that arise in Maxwell's equations Faraday's and Ampere's Laws. This algorithm is commonly know as the Finite Difference Time Domain Method (FDTD) [1, 2]. This method is probably one of the most popular methods in computational electrodynamics. However at times this method can become quite expensive computational wise. Many times when given a large computational domain with small structures present, the cost of resolving these structures require a lot of computer storage which increases the computation time. Other numerical techniques have also been used to solve these equations such as, method of moments (MOM), finite element method (FEM) [3], and hybrid implicit-explicit finite difference time domain method [4]. We chose this method because of the level of accuracy in which it achieves while having its simplicity in implementation. A lot of extensive research has been done with the FDTD method in regards to solving the Maxwell's equations. Researchers modeled different types of materials using this method.

In this work we present a novel local mesh refinement algorithm based on the use of transformation optics [5]. We solve Maxwell's equations using the FDTD method through a coordinate transformation. Transformation optics (TO) is a method that can control the propagation of light due to the invariance of Maxwell's equations under a geometrical transformation [7]. Transformation optics has found wide applications in designing novel electromagnetic (EM) devices such as invisibility cloaks, hyper-lens, waveguides, and superscatterers [7]. Researchers in optics have shown great interest in the field of transformation optics (TO) because of the ability to control the electromagnetic fields into needed spatial patterns and to support surface plasmon polariton surface waves [3]. Transformation optics has successfully provided analytical solutions to various problems in plasmonics. Its potential resides in its ability to relate highly symmetric structures to more complex ones [6]. The TO method maps the original geometry into a more symmetric geometry which improves the efficiency and gives more physical insight through revealing hidden symmetries [8]. One of the major advantages of the TO method is the proven stability property of the numerical methods applied to the anisotropic Maxwell's equations. In comparison to the standard FDTD method, the TO method shows significant improvement of efficiency without losing accuracy. One example shown [5] is the resolving of a metallic bow tie structure with a small gap of $10 \sim nm$, the TO-FDTD method speeds up the simulation for more than 300 times.

One of the applications we will consider in this work is the modeling of superscattering of dispersive materials. Superscattering is a phenomenon of the nanoparticles with scattering cross section from a subwavelength object exceeding the single channel limit[9]. Graphene is a one atom thick layer of carbon atoms arranged in a honeycomb lattice that has unique optical features and optoelectronic properties [6]. One of the most interesting features of graphene is that its conductivity and permittivity can be tuned by a biasing electrostatic or magnetostatic field and it can support highly confined surface plasmon polariton (SPP) surface waves [3]. More interesting properties of graphene are magnetically induced gyrotropy, its linear dispersion characteristic, which results in high electron mobility not achievable in semiconductors, and the tunability of its conductivity due to a specific hybridization that produces unoccupied atomic orbitals vertical to the graphene surface [10]. In chapter two, we give a more conceptual description of Maxwell's equations along with its constitutive relations. We show how the Finite-Difference Time Domain method discretizes these equations and how update equations are derived. We then show how these equations model incident plane waves in one dimension and two dimensional spaces. We also discuss an absorbing boundary condition commonly referred to as The Perfectly Matching Layer (PML) Boundary. After discussing the PML boundary we show how the FDTD method can model dispersive material. Chapter three is where we introduce The Transformation Optics method. We first give an introduction of the method by giving a brief history on how the TO can be adopted in the FDTD Maxwell solver to improve efficiency. We then discuss the steps of the TO based Maxwell's solver and the coordinate transformation that is made to change a certain region in a given material and how the TO method can model dispersive material. Chapter 4 shows the numerical simulations and the comparisons of the standard FDTD method and the TO method. Finally chapter five is the conclusion.

1.2 Literature Review

Superscattering of Light from Subwavelength Nanostructures: Ref [13] shows that a superscatterer could be design by creating resonance in large numbers of channels by making sure that the resonances all operate in the strong over coupling limit and also aligning the different resonant frequencies. When a sub-wavelength object is a single atom in a three dimensional vacuum, its scattering cross section is $\frac{(2l+1)\lambda^2}{2\pi}$ at the atomic resonant frequency, where l is the total angular frequency. This limit becomes $\frac{3\lambda^2}{2\pi}$ for a given typical electric dipole transition. A nanorod which consisted of multiple concentric layers of dielectric and plasmonic materials was considered. The plasmonic material is described by the Drude model with $\epsilon = 1 - \dfrac{\omega_p^2}{\omega^2 + i\gamma_d\omega}$, where ϵ is the relative permittivity, ω_p is the plasma frequency, ω is the incident frequency, and γ is the damping term. They were able to show that the maximum single channel limit of a particle's cross section could be enhanced significantly whether loss was present or not. The first case is the loss less case. In the loss less case $\gamma_d = 0$, it is shown that the resonance of the nanorod satisfies the whispering gallery condition. So for a given plasma frequency the single channel limit is enhanced by more than two times the given single channel limit. In the lossy case, the damping term γ_d takes into account the bulk and the surface scattering effect. For the same given plasma frequency the single channel limit is still enhance by at least two times the single channel limit.

Tunable deep-sub wavelength superscattering using graphene monolayers: In [14] graphene monolayers are used for the first time to design a superscatterer. This work shows that sub wavelength objects can be scaled down to deep-sub-wavelength objects and their scattering cross sections become extremely far below the single channel limit and the original structures can not be scaled down directly for superscattering purposes. It was proposed that a layer of graphene be added to the dielectric material to design the superscatterer. By adding a layer of graphene to the material they were able to enhance the scattering cross section of a particle by six orders of magnitude. The applicability for dielectric media with different permittivities and different incident frequencies are analyzed by utilizing the tunability of surface conductivity of graphene. A transverse magnetic polarized incident plane wave normally incidents onto an infinite graphene coated cylindrical dielectric medium is considered. The surface conductivity of graphene is what is modeled. The surface conductivity is modeled the Kubo's formula

$\sigma_g(\omega, \mu_c, \Gamma, T) = \sigma_{intra} + \sigma_{inter}$ where

$$\sigma_{intra} = \frac{ie^2 k_b T}{\pi \hbar^2 (\omega + i2\Gamma)} \left[\frac{\mu_c}{k_B T} + 2\ln(e^{-\frac{\mu_c}{k_B T}} + 1) \right],$$

is due to intraband and

$$\sigma_{inter} = \frac{ie^2(\omega + i2\Gamma)}{\pi \hbar^2} \int_0^{\infty} \frac{f_d(-\epsilon) - f_d(\epsilon)}{(\omega + i2\Gamma)^2 - 4\left(\frac{\epsilon}{\hbar}\right)^2} d\epsilon,$$

is due to interband where $-e$ is the charge of an electron, $\hbar = \dfrac{h}{2\pi}$ is the reduced Plank's constant, $\omega = 2\pi f$ is the angular frequency of the incident field, Γ is the phenomenological scattering rate that is assumed to be independent of the energy ϵ $f_d(\epsilon) = \dfrac{1}{(e^{(\epsilon - \mu_c)/k_B T} + 1)}$ is the Fermi Dirac distribution, k_B is the Boltzmann's constant, T is the temperature and μ_c is the chemical potential that can be tuned by a gate voltage. Finally they show that the two conditions are satisfied to achieve superscattering. First is the tuning of the permittivity, where the coating layer was determined to satisfy this condition. The tuning of the permittivity is one of graphene's most interesting features and the second one was optical loss was determined by the coating layer being small enough to satisfy this condition.

An FDTD Model of Graphene Intraband Conductivity; Ref [10] shows a model of magnetized graphene gyrotropic conductivity in this work. It is shown on the basis of equivalent circuit representation that a static magnetic bias changes a Drude dispersion characteristics of graphene into an extended Lorentz model supplemented with an additional barانch accounting for the induced gyrotropy. The most common representation of graphene is based on a Drude conductivity model

$$\sigma_D = \sigma_0 \frac{1}{1 + j\omega\tau}$$

which is frequently applied to the modeling of conductive materials at high frequencies. Intraband conductivity of graphene can be accurately represented by,

$$\sigma_{xx} = \sigma_0 \frac{1 + j\omega\tau}{(\omega_c\tau)^2 + (1 + j\omega\tau)^2} \tag{1.1}$$

$$\sigma_{yx} = \sigma_0 \frac{1 + j\omega\tau}{(\omega_c\tau)^2 + (1 + j\omega\tau)^2}, \tag{1.2}$$

where xx, (yx) denotes a diagonal (off diagonal) component of a two dimensional conductivity tensor, σ_0 is the static conductivity, τ is the scattering time, and ω_c is the cyclotron frequency. An ADE-FDTD model of intraband conductivity of magnetized graphene is developed and validated by computational examples in this paper.

Interactions between graphene-coated nanowires revisited with transformation optics: Ref [8] studies the interaction between two dielectric-core graphene shell nanowirers. The scattering and absorption as well as the field distributions are analytically derived. The results are polarization independent multi-frequency Fanodips. The localized surface plasmon modes of single graphene-coated nanowires can interact with each other to form pairs of bonding and anti-bonding modes, which will further split apart when increasing the coupling strength. Drawbacks are an analytical solution of the optical response of a two dimensional core-shell dimer can be obtained by using Mie scattering theory, however this strategy involves higher-order cylindrical harmonics whose treatment can be computationally consuming. By mapping the original geometry to a more symmetric geometry, the efficiency is improved and more physical insights are gained through hidden symmetry. Indium antimonide is chosen in the calculations as a counterpart to graphene for its small energy band gap and large electronic mobility. The traditional transformation theory cannot be applied to graphene coated structures because, unlike the in-plane permittivity, the conductivity of graphene is no longer preserved under the transformation. So they define a conformal mapping. Under this conformal map the in-plane components of the electric permittivity are conserved. A spatially dependent conductivity of graphene is introduced in the transformed frame. It shown that this spatial dependence may break rotational symmetry in the transformation but, it only causes minor complications to the problem. A dimer system is transformed into an annular system with much more symmetry. It is assumed that the cores of the dimer are comprised of homogeneous dielectrics defined by a permittivity ϵ_s. The conductivity of the graphene is spatially variant in the transform but, that independence is eliminated by the deriving of a tridiagonal system of equations. Once this is done then system is validated through numerical simulations.

Transformation Optics Using Graphene: In Ref [18], Noble metals like silver and gold have been used many times in the past to construct optical metamaterials. However, problems arise when it became difficult to control the permittivity of the metals and the existence of high material loss. These drawbacks degrade the quality of plasmon resonance and limit the relative propagation lengths of surface polariton plasmon waves. This puts a constraint on the functionality of the metamaterials and transfomation optical devices. Ref [18] shows that graphene can serve as a platform for metamaterials and transformation optical devices. It is shown that with the proper choice of conductivity, spatial patterns across the graphene provide exciting possibilities for tailoring, manipulating, and scattering IR SPP wave signals across the graphene. With the given parameters $T = 3K$ $\Gamma = 0.43meV$ and $\mu_c = 0.15ev$ where T is the temperature, Γ is the scattering rate, and μ_c is the chemical potential, the highly compressed mode offers an effective SPP index of 69.34. A SPP surface wave to reflect or refract on this sheet of graphene can be engineered.

Dispersion HIE-FDTD method for simulating graphene based absorber: In Ref.[4] a graphene based absorber is designed by a new hybrid implicit-explicit (HIE-FDTD) method. A few improved methods have be proposed to design this graphene device but as the Courant-Friedrich-Levy (CFL) stability condition is mainly limited by the smallest cell, these methods become computationally expensive when they are used to simulate these devices. The time step size of this method is only related to two space discretizations instead of the smallest one. In one example it is shown where using the standard FDTD method to model a graphene based absorber device took approximately $17Ks$ where as with the dispersion HIE-FDTD method it only took $2s$ and the final example the standard FDTD method takes approximately $85Ks$ whereas the dispersion HIE-FDTD method only took $100s$. So clearly this method is accurate and can reduce the amount of computational time significantly. In this method, graphene is treated as an infinitesimally thin conducting surface. Since graphene is a dispersive medium, the ADE method is used to assist in the deriving of the update equations. Once these update equations are derived the graphene based absorber is simulated and the efficiency is validated through the comparison of time.

A Simple FDTD approach for The Analysis and Design of Graphene Based Optical Devices: In Ref. [3] for the first time the Maxwell curl equations with a normalized flux density in the FDTD method are used to simulate graphene material. No modification is needed for the graphene conductivity in the curl equations because the equations become independent of the material. The normalized flux density becomes a function of frequency as the conductivity and permittivity of graphene is frequency dependent. Graphene is modeled by a surface conductivity equation. The conductivity in Maxwell's equations is associated as volumetric conductivity instead of surface conductivity. Volumetric conductivity is calculated from surface conductivity divided by the thickness of a graphene sheet. The curl equations are expressed in the normalized flux density instead of the electric field because the current density creates more computational expensive and the equations get into a more difficult form with the graphene conductivity which is a non-linear function of frequency.

Tunable Invisibility Cloaking Using Isolated Graphene Coated Nanowires and Dimers: Ref [20] finds that to reduce the scattered signal from subwavelength particles, materials need an extremal value of the permittivity/permeability. Graphene possesses these characteristics for the use in optoelectronic devices in the infrared and terahertz region because of the ability to mold the surface current with low loss. A lot of different methods have been proposed with plasmonic compounds, using a dipole moment of opposite phase to attain a scattering cancellation, so this Ref [20] they extend the previous concept by employing a p-polarized incident plane wave that illuminates a graphene coated dielectric nanowire in order to get near the fundamental localized surface plasmon polariton. They look at the illumination of a graphene coated nano-cylinder by a plane electromagnetic wave in the far infrared range of frequencies. An analytical formula is derived for fast evaluation of the spectral window with a significantly reduction in scattering efficiency for a sufficiently thin cylinder. As a result, this polarization dependent effect leads to a tunable resonant invisibility that can be achieved by a modification of the grahene chemical potential monitored by a gate voltage.

Design of Ultra-Compact Graphene-Based Superscatterers: In [19] they show how the method of dispersion engineering can be used to design an ultra-compact graphene based superscatterer. Many approaches have been taken to design these types of superscatterers such as the overlapping of multiple resonances. First it is shown that the applicability of the Bohr model to graphene based structures is shown by taking the dielectric graphene air cylindrical structure as an example,next they sow the validation of the Bohr model when multiple dispersion curves exist simultaneously. The resonance peaks from the first and second order scattering terms are overlapped by engineering the dispersion relation of the equivalent plasmon waveguide. Finally they design the superscatterer by the dispersion engineering.

Design of a Sub wavelength Superscattering Nanoshpere: Ref [21] talks about designing a superscattering nanosphere with a plasmonic-dielectric-plasmonic layer structure. This paper shows that the scattering cross section of such a particle can be enhanced significantly by employing multiple resonances with different total angular momenta, and by ensuring that all these resonances have almost the same frequency and operate in the same over coupling region.many applications stem from the enhancing of the scattering cross section of a subwavlength nanoparticle such as imaging, bio medicine, and photovoltaics. Prior strategies in this design included creating a resonance in channels with high total angular momentum, however this work sought to create an accidental degeneracy of the resonant modes with different total angular momenta. The advantage to this is that you can exploit the channels with a smaller total angular momentum because they are typically less susceptible to loss and more stably stay in the over coupling region. In a previous work of these authors, in designing a superscatterer, a nanorod was considered that consisted of concentric metal-dielectric-metal layer. The metal is describe by the Drude model

$$\epsilon_m = 1 - \frac{\omega_p^2}{\omega^2 + i\gamma_d\omega}.$$

Here in this work they show that this idea can be extended to a three dimensional case. Similar to their previous work, they first investigate the loss less case where $\gamma_d = 0$, here in the nanosphere the resonances are of the whispering gallery and the modes are all degenerate, therefore the planar structure will change into near degeneracy in the nanosphere between modes of different angular moment.

Chapter 2

FDTD METHOD

2.1 Maxwell's Equation

Maxwell's Equations [1] are a set of differential equations which govern electromagnetic wave propagation through vacuum and matter. These equations are composed of the electric field, the magnetic field, the electric flux density, and the magnetic flux density. Constitutive relations define the relationships between the electric field, and the electric flux density, the magnetic field, and the magnetic flux density. These relations show how the electric field and the magnetic field relate to different sources, charge densities, and current densities. In addition to that, they show their interaction with other materials and how they develop with time. Maxwell's equations are known as Gauss's Law, Gauss's Law for Magnetism, Faraday's Law, and Ampere's Law. Gauss's Law shows how the electric field and the electric charges that are generated are related. Electric fields diverge from positive charges and converge on negative charges. If there are no charges then the electric field will just form loops. Guass's Law for Magnetism says that there is no relationship between electric charges and magnetic charges but rather the magnetic field is mainly generated by a dipole that has no magnetic charge at all. The magnetic field always form loops. Furthermore, Faraday's Law states that a changing magnetic field can induce an electric field. Conversely, an induced electric field can create a change in the magnetic field. Ampere's Law states that the magnetic field can be generated by an electric current.
The time-dependent Maxwell's equations are as follows [1],
Faraday's Law,

$$\frac{\partial \vec{B}}{\partial t} = - \bigtriangledown \times \vec{E}, \tag{2.1}$$

Ampere's Law,

$$\frac{\partial \vec{D}}{\partial t} = \bigtriangledown \times \vec{H}, \tag{2.2}$$

Gauss's Law,

$$\bigtriangledown \cdot \vec{D} = \rho, \tag{2.3}$$

Gauss's Law for Magnetism,

$$\bigtriangledown \cdot \vec{B} = 0. \tag{2.4}$$

Here $\vec{E}$ is the electric field in volts per meter, $\vec{D}$ is the electric flux density in coulombs per square meter, $\vec{H}$ is the magnetic field in amperes per meter, $\vec{B}$ is the magnetic flux density in weberes per square meter, and ρ is the free charge density. These curl equations predict electromagnetic waves. The divergence equations and the curl equations are what produce the fields. Now for nondispersive, isotropic, linear material we can show the relationships between the electric field $\vec{E}$, and the electric flux density $\vec{D}$, the magnetic field $\vec{H}$, and the magnetic flux $\vec{B}$ as,

$$\vec{D} = \epsilon \vec{E}, \tag{2.5}$$

and

$$\vec{B} = \mu \vec{H}, \tag{2.6}$$

where μ is the permeability in henrys per meter and ϵ is the permittivity in farads per meter. These equations are the constitutive relations mentioned earlier. Constitutive relations show how the fields interact with materials. The permittivity is a measure of how well a material stores electric energy. A circulating magnetic field induces an electric field at the center of the circulation in proportion to the permittivity. The dielectric constant of a material is its permittivity relative to the permittivity of free space ϵ_0. The permeability is a measure of how well a material stores magnetic energy. A circulating electric field induces a magnetic field at the center of the circulation in proportion to the permeability. The relative permeability of a material is its permeability relative to the permeability of free space μ_0.

Now substituting (2.5) and (2.6) into (2.1) and (2.2) we get the following Maxwell's curl equations,

$$\mu\frac{\partial\vec{H}}{\partial t} = -\bigtriangledown\times\vec{E}, \tag{2.7}$$

and

$$\epsilon\frac{\partial\vec{E}}{\partial t} = \bigtriangledown\times\vec{H}. \tag{2.8}$$

Note that each vector is a three dimensional vector. Therefore if we were to write out the vector components of the curl operators in (2.7) and (2.8) we would have six coupled scalar equations that are equivalent to the Maxwell's equations in three dimensions. These equations can be reduced to one dimensional and two dimensional equations by assuming that the fields are only dependent upon one or two space variables.

2.2 FDTD Method

The Finite Difference Time Domain (FDTD) method [1, 2] is a very popular method used to numerically solve Maxwell's Equation in the time domain using finite difference approximations. Its popularity is due to its simplicity, stability, and ability to easily couple a large variety of material models. The FDTD method employs finite differences as approximations to both the spatial and temporal derivatives that appear in Maxwell's equations. The FDTD method computes electric and magnetic fields on space-time staggered grids with centered difference and leap frog updates in the temporal domain. Key advantages of the FDTD method include divergence free and dissipation free.

Consider the Taylor series expansion of the function $f(x)$ expanded about the point x_0

with an offset of $\pm\dfrac{\delta}{2}$,

$$f\left(x_0+\frac{\delta}{2}\right)=f(x_0)+\frac{\delta}{2}f'(x_0)+\frac{1}{2!}\left(\frac{\delta}{2}\right)^2 f''(x_0)+\frac{1}{3!}\left(\frac{\delta}{2}\right)^3 f'''(x_0)+\ldots\quad, \tag{2.9}$$

$$f\left(x_0-\frac{\delta}{2}\right)=f(x_0)-\frac{\delta}{2}f'(x_0)+\frac{1}{2!}\left(\frac{\delta}{2}\right)^2 f''(x_0)-\frac{1}{3!}\left(\frac{\delta}{2}\right)^3 f'''(x_0)+\ldots\quad. \tag{2.10}$$

Subtracting the two equations, yields

$$f\left(x_0+\frac{\delta}{2}\right)-f\left(x_0-\frac{\delta}{2}\right)=\delta f'(x_0)+\frac{2}{3!}\left(\frac{\delta}{2}\right)^3 f'''(x_0)+\ldots\quad. \tag{2.11}$$

Now if we divide through by δ we obtain the following equation

$$\frac{f\left(x_0+\frac{\delta}{2}\right)-f\left(x_0-\frac{\delta}{2}\right)}{\delta}=f'(x_0)+\frac{1}{3!}\left(\frac{\delta}{2}\right)^2 f'''(x_0)+\ldots\quad. \tag{2.12}$$

From (2.12) we see that the left hand side of the equation is equal to the derivative of the function. We can denote the remaining terms as $O(\delta^2)$. Thus we have,

$$\left.\frac{df(x)}{dx}\right|_{x=x_0}=\frac{f\left(x_0+\frac{\delta}{2}\right)-f\left(x_0-\frac{\delta}{2}\right)}{\delta}+O(\delta^2). \tag{2.13}$$

Since the lowest power of δ being ignored is second order, the central difference has second-order accuracy or second-order behavior. This implies that if δ is reduced by a factor of 10, the error in the approximation should be reduced by a factor of 100. For a sufficiently small δ we can disregard the terms represented by $O(\delta^2)$ which will give us

$$\left.\frac{df(x)}{dx}\right|_{x=x_0}=\frac{f\left(x_0+\frac{\delta}{2}\right)-f\left(x_0-\frac{\delta}{2}\right)}{\delta}. \tag{2.14}$$

Taking the limit as $\delta \to 0$ we approach an exact solution. We have now obtained a second-order central difference.

The FDTD algorithm was first proposed by Kane Yee in 1966 for the lossless material case $\rho = 0$. The algorithm employs second-order central differences. The staggered location of the $\vec{E}$ and $\vec{H}$ components in the Yee grid and central difference operations on these components enforce the two Gauss's Law relations, therefore the mesh is divergence free with respect to its electric and magnetic fields and also enforces the absence of free electric and magnetic charge in the source free space being modeled [1]. The FDTD algorithm can be summarized as follows:

1. Replace all the derivatives in Ampere's Law and Faraday's Law with finite differences. Discretize space and time so that the electric and magnetic field are staggered in both space and time.

2. Solve the resulting difference equations to obtain update equations that express the future (unknown) fields in terms of the past (known) fields.

2a Evaluate (update) the magnetic fields one time-step into the future so they are now known.

2b Evaluate (update) the electric fields one time-step into the future so they are now known.

3. Repeat the previous two steps (2a & 2b) until the fields have been obtained over the desired duration.

2.2.1 FDTD In 1D

Consider the following transverse electromagnetic TEM mode z-polarized x-directed one dimensional Maxwell's equations,

$$\mu \frac{\partial H_y}{\partial t} = \frac{\partial E_z}{\partial x}, \tag{2.15}$$

and

$$\epsilon \frac{\partial E_z}{\partial t} = \frac{\partial H_y}{\partial x}. \tag{2.16}$$

Let

$$H_y^{n+\frac{1}{2}}\left[i+\frac{1}{2}\right] = H_y\left(t_0 + \left(n+\frac{1}{2}\right)\triangle t, x_0 + \left(i+\frac{1}{2}\right)\triangle x\right),$$

and

$$E_z^n\left[i\right] = E_z\left(t_0 + n\triangle t, x_0 + i\triangle x\right).$$

Replacing each derivative with finite differences we get,

$$\mu\left(\frac{H_y^{n+\frac{1}{2}}\left[i+\frac{1}{2}\right] - H_y^{n-\frac{1}{2}}\left[i+\frac{1}{2}\right]}{\triangle t}\right) = \frac{E_z^n\left[i+1\right] - E_z^n\left[i\right]}{\triangle x}, \tag{2.17}$$

and

$$\epsilon\left(\frac{E_z^{n+1}\left[i\right] - E_z^n\left[i\right]}{\triangle t}\right) = \frac{H_y^{n+\frac{1}{2}}\left[i+\frac{1}{2}\right] - H_y^{n+\frac{1}{2}}\left[i-\frac{1}{2}\right]}{\triangle x}. \tag{2.18}$$

Solving for $H_y^{n+\frac{1}{2}}\left[i+\frac{1}{2}\right]$ and $E_z^{n+1}\left[i\right]$ we get the following,

$$H_y^{n+\frac{1}{2}}\left[i+\frac{1}{2}\right] = H_y^{n-\frac{1}{2}}\left[i+\frac{1}{2}\right] + \frac{\triangle t}{\mu\triangle x}\left(E_z^n\left[i+1\right] - E_z^n\left[i\right]\right), \tag{2.19}$$

and

$$E_z^{n+1}\left[i\right] = E_z^n\left[i\right] + \frac{\triangle t}{\epsilon\triangle x}\left(H_y^{n+\frac{1}{2}}\left[i+\frac{1}{2}\right] - H_y^{n+\frac{1}{2}}\left[i-\frac{1}{2}\right]\right). \tag{2.20}$$

Thus equations (2.19) and (2.20) are update equations for the electric and magnetic field. Figure 2.1 shows an example of a one dimensional plane wave of the electric field

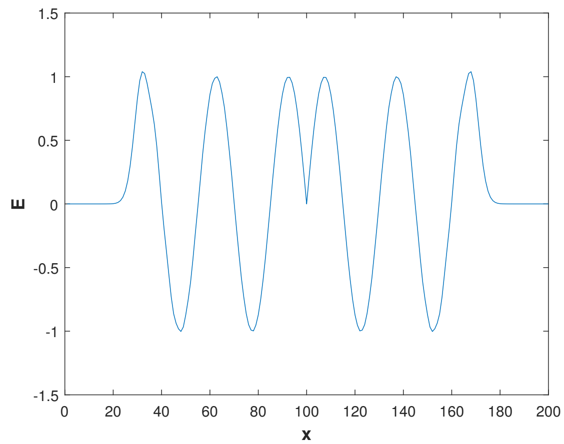

Figure 2.1: One dimensional plane wave of the electric field distribution

distribution in the x - direction. Max time is set to 300 steps. The incident source $E = \sin(\omega t)$ at the center of the domain with $\omega = \dfrac{2\pi c}{\lambda}$ is the power source inside a 200 grid point graph. $\triangle x = 0.1$, $\triangle t = \dfrac{\triangle x}{2 \cdot c}$, where c is the speed of light, $c = 3 \times 10^8 m/s$, $\epsilon_0 = 8.854 \times 10^{-12}$, $\mu_0 = 4\pi \times 10^{-7}$, and $\lambda = 3$.

2.2.2 FDTD in 2D

Now consider the two dimensional TEz mode Maxwell's equation

$$\epsilon \frac{\partial E_x}{\partial t} = \frac{\partial H_z}{\partial y}, \tag{2.21}$$

$$\epsilon \frac{\partial E_y}{\partial t} = -\frac{\partial H_z}{\partial x}, \tag{2.22}$$

and

$$\mu \frac{\partial H_z}{\partial t} = \frac{\partial E_x}{\partial y} - \frac{\partial E_y}{\partial x}. \tag{2.23}$$

Replacing each derivative with finite differences we get,

$$\epsilon\left(\frac{E_x^{n+1}\left[i+\frac{1}{2},j\right]-E_x^{n}\left[i+\frac{1}{2},j\right]}{\triangle t}\right)=\frac{H_z^{n+\frac{1}{2}}\left[i+\frac{1}{2},j+\frac{1}{2}\right]-H_z^{n+\frac{1}{2}}\left[i+\frac{1}{2},j-\frac{1}{2}\right]}{\triangle y}. \tag{2.24}$$

Solving for $E_x^{n+1}\left[i+\frac{1}{2},j\right]$ we get,

$$E_x^{n+1}\left[i+\frac{1}{2},j\right]=E_x^{n}\left[i+\frac{1}{2},j\right]+\frac{\triangle t}{\epsilon\triangle y}\left(H_z^{n+\frac{1}{2}}\left[i+\frac{1}{2},j+\frac{1}{2}\right]-H_z^{n+\frac{1}{2}}\left[i+\frac{1}{2},j-\frac{1}{2}\right]\right). \tag{2.25}$$

Similarly for E_y and H_z we get,

$$E_y^{n+1}\left[i,j+\frac{1}{2}\right]=E_y^{n}\left[i,j+\frac{1}{2}\right]+\frac{\triangle t}{\epsilon\triangle x}\left(H_z^{n+\frac{1}{2}}\left[i+\frac{1}{2},j+\frac{1}{2}\right]-H_z^{n+\frac{1}{2}}\left[i-\frac{1}{2},j+\frac{1}{2}\right]\right), \tag{2.26}$$

$$\begin{aligned}H_z^{n+\frac{1}{2}}\left[i+\frac{1}{2},j+\frac{1}{2}\right]=H_z^{n+\frac{1}{2}}\left[i+\frac{1}{2},j+\frac{1}{2}\right]&+\frac{\triangle t}{\mu}\left(\frac{E_x^{n+1}\left[i+\frac{1}{2},j+1\right]-E_x^{n+1}\left[i+\frac{1}{2},j\right]}{\triangle y}\right)\\&-\frac{\triangle t}{\mu}\left(\frac{E_y^{n+1}\left[i+1,j+\frac{1}{2}\right]-E_y^{n+1}\left[i,j+\frac{1}{2}\right]}{\triangle x}\right).\end{aligned} \tag{2.27}$$

Hence (2.25) – (2.27) are two dimensional update equations for Maxwell's equations. Figure 2.2 shows a two dimensional magnetic field's distribution in free space in the $x-y$ plane. Max time is set to 100 steps. The incident source $H=\sin(\omega t)$ at the center of the domain with $\omega=\dfrac{2\pi c}{\lambda}$ is the power source inside a 200 grid point graph. $\triangle x=\triangle y=0.1$, $\epsilon_0=8.854\times10^{-12}$, $\mu_0=4\pi\times10^{-7}$, $\triangle t=\dfrac{\triangle x}{2\cdot c}$, and $\lambda=3$.

2.3 Perfectly Matched Layer (PML) Boundary

When discussing the Perfectly Matched Layer (PML) boundary one must first introduce lossy material. Lossy material is the material with a finite conductivity. A conduction current term is then added to the Maxwell's equations. Consider the following one

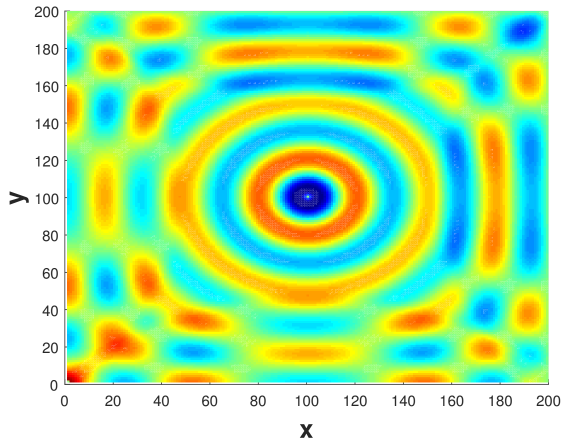

Figure 2.2: Two dimensional magnetic field distribution

dimensional Maxwell's equations

$$\mu\frac{\partial H_y}{\partial t} = \frac{\partial E_z}{\partial x}, \tag{2.28}$$

and

$$\epsilon\frac{\partial E_z}{\partial t} = \frac{\partial H_y}{\partial x}. \tag{2.29}$$

When loss is present we have,

$$\mu\frac{\partial H_y}{\partial t} + \sigma^* H_y = \frac{\partial E_z}{\partial x}, \tag{2.30}$$

and

$$\epsilon\frac{\partial E_z}{\partial t} + \sigma E_z = \frac{\partial H_y}{\partial x}, \tag{2.31}$$

where σ and σ^* represent the possible electric conductivity and the magnetic loss assigned to free space. To approximate the undifferentiated E field at $n+\frac{1}{2}$ we just take the average of the electric field on either side of the desired point. For example

$$E_x^{n+\frac{1}{2}}\left[i\right] = \frac{E_z^{n+1}\left[i\right] + E_z^{n}\left[i\right]}{2}. \tag{2.32}$$

Discretizing (2.32) and (2.33) we obtain the following,

$$\mu \left(\frac{H_y^{n+\frac{1}{2}}\left[i+\frac{1}{2}\right] - H_y^{n-\frac{1}{2}}\left[i+\frac{1}{2}\right]}{\triangle t} \right) + \sigma^* \left(\frac{H_y^{n+\frac{1}{2}}\left[i+\frac{1}{2}\right] + H_y^{n-\frac{1}{2}}\left[i+\frac{1}{2}\right]}{2} \right) = \left(\frac{E_z^n\left[i+1\right] - E_z^n\left[i\right]}{\triangle x} \right), \tag{2.33}$$

and

$$\epsilon \left(\frac{E_z^{n+1}\left[i\right] - E_z^n\left[i\right]}{\triangle t} \right) + \sigma \left(\frac{E_z^{n+1}\left[i\right] + E_z^n\left[i\right]}{2} \right) = \left(\frac{H_y^{n+\frac{1}{2}}\left[i+\frac{1}{2}\right] - H_y^{n+\frac{1}{2}}\left[i-\frac{1}{2}\right]}{\triangle x} \right). \tag{2.34}$$

Solving for $H_y^{n+\frac{1}{2}}\left[i+\frac{1}{2}\right]$ and $E_y^{n+1}\left[i\right]$ we obtain the two following update equations,

$$H_y^{n+\frac{1}{2}}\left[i+\frac{1}{2}\right] = \frac{1-\frac{\sigma^*\triangle t}{2\mu}}{1+\frac{\sigma^*\triangle t}{2\mu}} H_z^{n-\frac{1}{2}}\left[i+\frac{1}{2}\right] + \frac{\frac{\triangle t}{\mu\triangle x}}{1+\frac{\sigma^*\triangle t}{2\mu}} \left(E_z^n\left[i+1\right] - E_z^n\left[i\right]\right), \tag{2.35}$$

and

$$E_z^{n+1}\left[i\right] = \frac{1-\frac{\sigma\triangle t}{2\epsilon}}{1+\frac{\sigma\triangle t}{2\epsilon}} E_z^n\left[i\right] + \frac{\frac{\triangle t}{\epsilon\triangle x}}{1+\frac{\sigma\triangle t}{2\epsilon}} \left(H_y^{n+\frac{1}{2}}\left[i+\frac{1}{2}\right] - H_y^{n+\frac{1}{2}}\left[i-\frac{1}{2}\right] \right). \tag{2.36}$$

Figure 2.3 shows a one dimensional plane wave with a PML boundary of the electric field's distribution in the x - direction. Max time is set to 1000 time steps. The incident source $E = sin\left(\omega t\right)$ at the center, with $\omega = \dfrac{2\pi c}{\lambda}$ is a power source inside a 200 grid point cell. $\epsilon = 8.854 \times 10^{-12}$, $\mu = 4\pi \times 10^{-7}$, $c = 3 \times 10^8$, $\lambda = 3$, $\triangle x = 0.1$, $\triangle t = \dfrac{dx}{2c}$. The PML size is $10\triangle x$, and $\sigma_{max} = 320 \cdot \eta_0$ where $\eta_0 = \sqrt{\frac{\epsilon}{\mu}}$. The waves are being absorbed in the PML layer.

Now lets look at the two dimensional case of the PML boundary. To get a perfectly matched layer (PML) between a lossless region and a lossy region Berenger proposed a non physical anisotropic material known as the perfect matched layer (PML). In a PML there

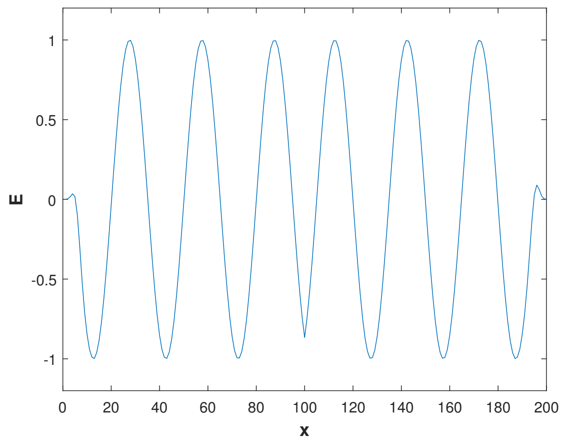

Figure 2.3: One dimensional plane wave with PML boundary on both ends

is no loss in the direction tangential to the interface, but there is loss normal to the interface. Consider the following two dimensional Maxwell's equation with the conduction current term σ added.

$$\epsilon\frac{\partial E_x}{\partial t} + \sigma_y E_x = \frac{\partial H_z}{\partial y}, \tag{2.37}$$

$$\epsilon\frac{\partial E_y}{\partial t} + \sigma_x E_y = -\frac{\partial H_z}{\partial x}, \tag{2.38}$$

$$\mu\frac{\partial H_z}{\partial t} + \sigma^* H_z = \frac{\partial E_x}{\partial y} - \frac{\partial E_y}{\partial x}. \tag{2.39}$$

Thus discretizing the Maxwell's equation when loss is present yields,

$$\begin{aligned} \epsilon\left(\frac{E_x^{n+1}\left[i+\frac{1}{2},j\right] - E_x^{n}\left[i+\frac{1}{2},j\right]}{\triangle t}\right) + \sigma_y\left(\frac{E_x^{n+1}\left[i+\frac{1}{2},j\right] + E_x^{n}\left[i+\frac{1}{2},j\right]}{2}\right) \\ = \frac{H_z^{n+\frac{1}{2}}\left[i+\frac{1}{2},j+\frac{1}{2}\right] - H_z^{n+\frac{1}{2}}\left[i+\frac{1}{2},j-\frac{1}{2}\right]}{\triangle y}. \end{aligned} \tag{2.40}$$

Solving for E_x^{n+1} yields,

$$E_x^{n+1}\left[i+\frac{1}{2},j\right]=\frac{1-\frac{\sigma_y\triangle t}{2\epsilon}}{1+\frac{\sigma_y\triangle t}{2\epsilon}}E_x^n\left[i+\frac{1}{2},j\right]+\frac{\frac{\triangle t}{\epsilon\triangle y}}{1+\frac{\sigma_y\triangle t}{2\epsilon}}\left(H_z^{n+\frac{1}{2}}\left[i+\frac{1}{2},j+\frac{1}{2}\right]\right)$$
$$-\frac{\frac{\triangle t}{\epsilon\triangle y}}{1+\frac{\sigma_y\triangle t}{2\epsilon}}\left(H_z^{n+\frac{1}{2}}\left[i+\frac{1}{2},j-\frac{1}{2}\right]\right). \tag{2.41}$$

When σ is zero this reduces to (2.25). Similarly for E_y^{n+1} we have,

$$E_y^{n+1}\left[i,j+\frac{1}{2}\right]=\frac{1-\frac{\sigma_x\triangle t}{2\epsilon}}{1+\frac{\sigma_x\triangle t}{2\epsilon}}E_y^n\left[i,j+\frac{1}{2}\right]+\frac{\frac{\triangle t}{\epsilon\triangle x}}{1+\frac{\sigma_x\triangle t}{2\epsilon}}\left(H_z^{n+\frac{1}{2}}\left[i+\frac{1}{2},j+\frac{1}{2}\right]\right)$$
$$-\frac{\frac{\triangle t}{\epsilon\triangle x}}{1+\frac{\sigma_x\triangle t}{2\epsilon}}\left(H_z^{n+\frac{1}{2}}\left[i-\frac{1}{2},j+\frac{1}{2}\right]\right). \tag{2.42}$$

Here σ_x is a function of x and σ_y is a function of y, so what Berenger proposed was to split either the electric field and/or the magnetic field into two components. To get the field all he did was add the two components together. In our case we split the magnetic field. Consider the following equation:

$$H_z = H_{zx} + H_{zy}. \tag{2.43}$$

Substituting (2.43) into (2.39) we obtain the following equation,

$$\mu\frac{\partial\left(H_{zx}+H_{zy}\right)}{\partial t}+\sigma^*\left(H_{zx}+H_{zy}\right)=\frac{\partial E_x}{\partial y}-\frac{\partial E_y}{\partial x}. \tag{2.44}$$

Next we split this equation into two equations with respect to each partial derivative.

$$\mu\frac{\partial H_{zx}}{\partial t}+\sigma_x^*H_{zx}=-\frac{\partial E_y}{\partial x}, \tag{2.45}$$

and

$$\mu\frac{\partial H_{zy}}{\partial t}+\sigma_y^*H_{zy}=\frac{\partial E_x}{\partial y}. \tag{2.46}$$

Discretizing the following equations we get,

$$H_{zx}^{n+\frac{1}{2}}\left[i+\frac{1}{2},j+\frac{1}{2}\right]=\frac{1-\frac{\sigma_x^*\triangle t}{2\mu}}{1+\frac{\sigma_x^*\triangle t}{2\mu}}H_{zx}^{n-\frac{1}{2}}\left[i+\frac{1}{2},j+\frac{1}{2}\right]-\frac{\frac{\triangle t}{\mu\triangle x}}{1+\frac{\sigma^*\triangle t}{2\mu}}\left(E_y^{n+1}\left[i+1,j+\frac{1}{2}\right]-E_y^{n+1}\left[i,j+\frac{1}{2}\right]\right), \tag{2.47}$$

and

$$H_{zy}^{n+\frac{1}{2}}\left[i+\frac{1}{2},j+\frac{1}{2}\right]=\frac{1-\frac{\sigma_y^*\triangle t}{2\mu}}{1+\frac{\sigma_y^*\triangle t}{2\mu}}H_{zy}^{n-\frac{1}{2}}\left[i+\frac{1}{2},j+\frac{1}{2}\right]+\frac{\frac{\triangle t}{\mu\triangle y}}{1+\frac{\sigma^*\triangle t}{2\mu}}\left(E_x^{n+1}\left[i+1,j+\frac{1}{2}\right]-E_x^{n+1}\left[i,j+\frac{1}{2}\right]\right). \tag{2.48}$$

Then to get the actual field we sum up the two components using (2.43).

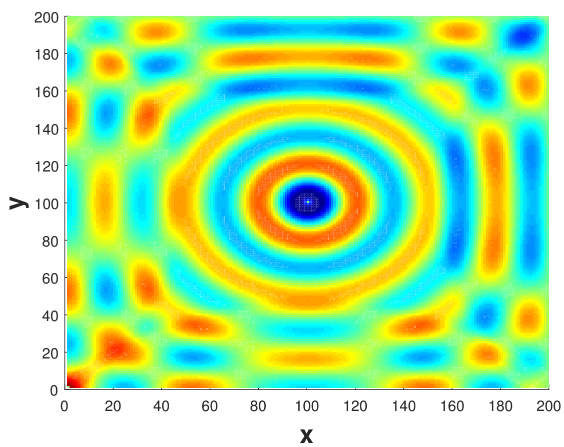

(a)

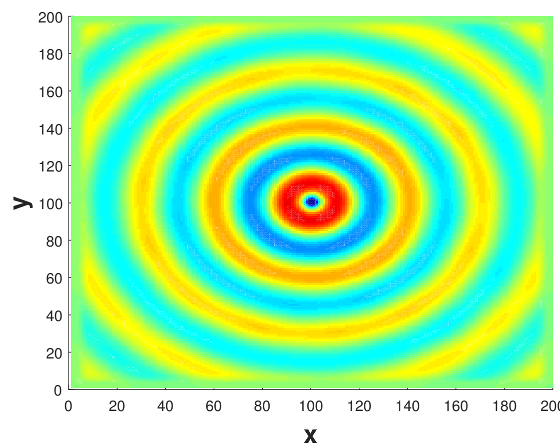

(b)

Figure 2.4: (a) Two dimensional plane wave of the magnetic field distribution without PML boundary, (b) with PML boundary

Figure 2.4 shows a two dimensional plane wave with a PML boundary of the magnetic field's distribution H_z which is the sum of the two equations (2.49) and (2.50) propagating through free space in the $x-y$ plane. Max time is set to 300 time steps. The incident source is $H = sin\,(\omega t)$ at the center of the domain is the power source inside a 200 grid point graph. $\epsilon = 8.854 \times 10^{-12}$, $\mu = 4\pi \times 10^{-7}$, $c = 3 \times 10^8$, $\lambda = 3$, $\omega = 2\pi \frac{c}{\lambda}$, $\triangle x = 0.1$, and $\triangle t = \frac{dx}{2c}$. PML size is $10\triangle x$ and $\sigma = 320 \cdot \eta_0$ where $\eta_0 = \sqrt{\frac{\epsilon}{\mu}}$. The reflection by the PML layer is about 10^{-4}.

2.4 Dispersive Material

In this section we study the interactions between electromagnetic waves and dispersive materials. In doing so it is very important to explain how a time domain differential equation that relates the electric flux density $D(r,t)$ to the electric field $E(r,t)$ is developed. In Maxwell's equations, where the material is non dispersive, the permittivity ϵ is independent of frequency. Thus we take Maxwell's equations and we discretize them using Yee's central differencing scheme in time and in space. However for dispersive material we have $\epsilon = \epsilon(\omega)$ where ω is the angular frequency. As stated earlier, we know that the constitutive relations show the relationship between the electric flux density, and the electric field, the magnetic flux density, and the magnetic field. Here we have the following constitutive relation equations [22],

$$D = \epsilon_0 E + P, \tag{2.49}$$

and

$$B = \mu_0(H + M), \tag{2.50}$$

where P and M are the electric and magnetic dipoles induced in the media and polarization vectors. These vectors can be related to the electric and magnetic field through an electric or magnetic susceptibility χ_e. Knowing this we can write the following,

$$\vec{P}(\omega) = \epsilon_0 \vec{\chi_e}(\omega)\vec{E}(\omega), \tag{2.51}$$

and

$$\vec{M}(\omega) = \vec{\chi_m}(\omega)\vec{H}(\omega), \tag{2.52}$$

giving us the following,

$$\vec{D}(\omega) = \epsilon_0 \vec{E}(\omega) + \epsilon_0 \vec{\chi_e}(\omega)\vec{E}(\omega), \tag{2.53}$$

$$\vec{B}(\omega) = \mu_0 \vec{H}(\omega) + \mu_0 \vec{\chi}_m(\omega)\vec{H}(\omega). \tag{2.54}$$

The Drude model is a commonly used model of the behavior of conductors therefore we use this to model dispersive materials. The electric susceptibility for Drude materials is given by,

$$\chi_e(\omega) = -\frac{\omega_p^2}{\omega^2 - j\gamma\omega}, \tag{2.55}$$

and the relative permittivity for a Drude material can thus be written as,

$$\epsilon_r = \epsilon_\infty - \frac{\omega_p^2}{\omega^2 - j\gamma\omega}, \tag{2.56}$$

where ϵ_r is the relative permittivity and the constant ϵ_∞ is the effect of the charged material at high frequencies where the susceptibility function goes to zero, ω_p is the plasma frequency, ω is the incident frequency, and γ is the damping term. Here j is the imaginary unit. We can also write the electric susceptibility for Drude materials as

$$\chi_e(\omega) = \frac{\omega_p^2}{j\omega(j\omega + \gamma)}. \tag{2.57}$$

Now we have the associated polarization current as,

$$J_p = j\omega P = j\omega\epsilon_0 \frac{\omega_p^2}{j\omega(j\omega + \gamma)}. \tag{2.58}$$

Canceling the $j\omega$ we get the following equation,

$$J_p = \epsilon_0 \frac{\omega_p^2}{j\omega + \gamma} E. \tag{2.59}$$

Multiplying through by $(j\omega + \gamma)$ we get,

$$J_p j\omega + J_p \gamma = \epsilon_0 \omega_p^2 E, \tag{2.60}$$

and taking the inverse fourier transform we get,

$$\frac{\partial J_p}{\partial t} + \gamma J_p = \epsilon_0 \omega_p^2 E. \tag{2.61}$$

This method is referred to as the Auxillary Differential Equations (ADE) method .

The FDTD model with the frequency dependences for dispersion will keep its nature of the original dispersionless FDTD. Lets look at the one dimensional Maxwell's equations and this time we allow the existence of a conduction current term J, thus we have the following,

$$\frac{\partial H_y}{\partial t} = \frac{1}{\mu_0} \frac{\partial E_z}{\partial x}, \tag{2.62}$$

and

$$\epsilon \frac{\partial E_z}{\partial t} = \frac{1}{\epsilon_0} \frac{\partial H_y}{\partial x} - J_z. \tag{2.63}$$

Discretizing (2.63) we obtain the following,

$$\begin{aligned} \epsilon \left(\frac{E_z^{n+1}(i) - E_z^n(i)}{\triangle t} \right) + \sigma \left(\frac{E_z^{n+1}(i) + E_z^n(i)}{2} \right) \\ + J_z^{n+\frac{1}{2}}(i) = \frac{H_y^{n+\frac{1}{2}} \left[i + \frac{1}{2} \right] - H_y^{n+\frac{1}{2}} \left[i - \frac{1}{2} \right]}{\triangle x}. \end{aligned} \tag{2.64}$$

Solving (2.64) for $E_z^{n+1}(i)$ we get,

$$
\begin{aligned}
E_z^{n+1}(i) = \left(\frac{1-\frac{\sigma\triangle t}{2\epsilon}}{1+\frac{\sigma\triangle t}{2\epsilon}}\right) E_z^n(i) - \left(\frac{\frac{\triangle t}{\epsilon}}{1+\frac{\sigma\triangle t}{2\epsilon}}\right) J_z^{n+\frac{1}{2}}(i) \\
+ \left(\frac{\frac{\triangle t}{\epsilon\triangle x}}{1+\frac{\sigma\triangle t}{2\epsilon}}\right)\left(H_y^{n+\frac{1}{2}}\left[i+\frac{1}{2}\right] - H_y^{n+\frac{1}{2}}\left[i-\frac{1}{2}\right]\right)
\end{aligned}
\tag{2.65}
$$

Now we need to calculate $J_z^{n+\frac{1}{2}}$ by solving the ADE:

$$
\frac{\partial J_z}{\partial t} + \gamma J_z = \epsilon_0 \omega_p^2 E_z. \tag{2.66}
$$

Discretizing (2.66) yields,

$$
\frac{J_z^{n+\frac{1}{2}}(i) - J_z^{n-\frac{1}{2}}(i)}{\triangle t} + \gamma\left(\frac{J_z^{n+\frac{1}{2}}(i) - J_z^{n-\frac{1}{2}}(i)}{2}\right) = \epsilon_0 \omega_p^2 E_z^n(i). \tag{2.67}
$$

Solving (2.67) for $J_z^{n+\frac{1}{2}}(i)$ yields,

$$
J_z^{n+\frac{1}{2}}(i) = \left(\frac{1-\frac{\gamma\triangle t}{2}}{1+\frac{\gamma\triangle t}{2}}\right) J_z^{n-\frac{1}{2}}(i) + \left(\frac{\triangle t}{1+\frac{\gamma\triangle}{2}}\right)\epsilon_0\omega_p^2 E_z^n(i). \tag{2.68}
$$

Now consider Ampere's Law the two dimensional Maxwell's equations,

$$
\epsilon\frac{\partial E_x}{\partial t} + \sigma_y E_x + J_x = \frac{\partial H_z}{\partial y}, \tag{2.69}
$$

and

$$
\epsilon\frac{\partial E_y}{\partial t} + \sigma_x E_y + J_y = -\frac{\partial E_y}{\partial x}. \tag{2.70}
$$

Note that,

$$
J_z^{n+\frac{1}{2}}(i) = \left(\frac{1-\frac{\gamma\triangle t}{2}}{1+\frac{\gamma\triangle t}{2}}\right) J_z^{n-\frac{1}{2}}(i) + \left(\frac{\triangle t}{1+\frac{\gamma\triangle}{2}}\right)\epsilon_0\omega_p^2 E_z^n(i).
$$

The J_x and J_y update equations are,

$$J_x^{n+\frac{1}{2}}\left[i+\frac{1}{2},j\right]=\left(\frac{1-\frac{\gamma\triangle t}{2}}{1+\frac{\gamma\triangle t}{2}}\right)J_x^{n-\frac{1}{2}}\left[i+\frac{1}{2},j\right]+\left(\frac{\triangle t}{1+\frac{\gamma\triangle}{2}}\right)\epsilon_0\omega_p^2E_x^n\left[i+\frac{1}{2},j\right], \tag{2.71}$$

and

$$J_y^{n+\frac{1}{2}}\left[i,j+\frac{1}{2}\right]=\left(\frac{1-\frac{\gamma\triangle t}{2}}{1+\frac{\gamma\triangle t}{2}}\right)J_y^{n-\frac{1}{2}}\left[i,j+\frac{1}{2}\right]+\left(\frac{\triangle t}{1+\frac{\gamma\triangle}{2}}\right)\epsilon_0\omega_p^2E_y^n\left[i,j+\frac{1}{2}\right]. \tag{2.72}$$

Discretizing (2.69) we get,

$$\begin{aligned}\epsilon\left(\frac{E_x^{n+1}\left[i+\frac{1}{2},j\right]-E_x^n\left[i+\frac{1}{2},j\right]}{\triangle t}\right)+\sigma_y\left(\frac{E_x^{n+1}\left[i+\frac{1}{2},j\right]+E_x^n\left[i+\frac{1}{2},j\right]}{2}\right)\\+J_x^{n+\frac{1}{2}}\left[i+\frac{1}{2},j\right]=\frac{H_z^{n+\frac{1}{2}}\left(i+\frac{1}{2},j+\frac{1}{2}\right)-H_z^{n-\frac{1}{2}}\left(i+\frac{1}{2},j-\frac{1}{2}\right)}{\triangle y}.\end{aligned} \tag{2.73}$$

Solving (2.73) for $E_x^{n+1}(i,j)$ we get,

$$\begin{aligned}E_x^{n+1}\left[i+\frac{1}{2},j\right]=\left(\frac{1-\frac{\sigma_y\triangle t}{2\epsilon}}{1+\frac{\sigma_y\triangle t}{2\epsilon}}\right)E_x^n\left[i+\frac{1}{2},j\right]-\left(\frac{\frac{\triangle t}{\epsilon\triangle y}}{1+\frac{\sigma\triangle t}{2\epsilon}}\right)J_x^{n+\frac{1}{2}}\left[i+\frac{1}{2},j\right]\\+\left(\frac{\frac{\triangle t}{\epsilon\triangle y}}{1+\frac{\sigma\triangle t}{2\epsilon}}\right)\left(\frac{H_z^{n+\frac{1}{2}}\left(i+\frac{1}{2},j+\frac{1}{2}\right)-H_z^{n+\frac{1}{2}}\left(i+\frac{1}{2},j-\frac{1}{2}\right)}{\triangle y}\right).\end{aligned} \tag{2.74}$$

Similarly for (2.70) we get the following update equation for E_y,

$$\begin{aligned}E_y^{n+1}\left[i,j+\frac{1}{2}\right]=\left(\frac{1-\frac{\sigma_x\triangle t}{2\epsilon}}{1+\frac{\sigma_x\triangle t}{2\epsilon}}\right)E_y^n\left[i,j+\frac{1}{2}\right]-\left(\frac{\frac{\triangle t}{\epsilon\triangle x}}{1+\frac{\sigma_x\triangle t}{2\epsilon}}\right)J_y^{n+\frac{1}{2}}\left[i,j+\frac{1}{2}\right]\\+\left(\frac{\frac{\triangle t}{\epsilon\triangle x}}{1+\frac{\sigma_x\triangle t}{2\epsilon}}\right)\left(\frac{H_z^{n+\frac{1}{2}}\left(i+\frac{1}{2},j+\frac{1}{2}\right)-H_z^{n+\frac{1}{2}}\left(i+\frac{1}{2},j-\frac{1}{2}\right)}{\triangle x}\right).\end{aligned} \tag{2.75}$$

Figure2.5 shows one dimensional pulse propagating through dispersive materal in the $x-$

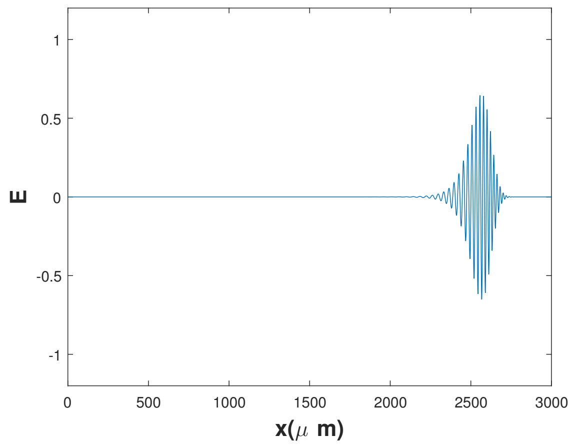

Figure 2.5: One dimensional pulse propagation in dispersive material.

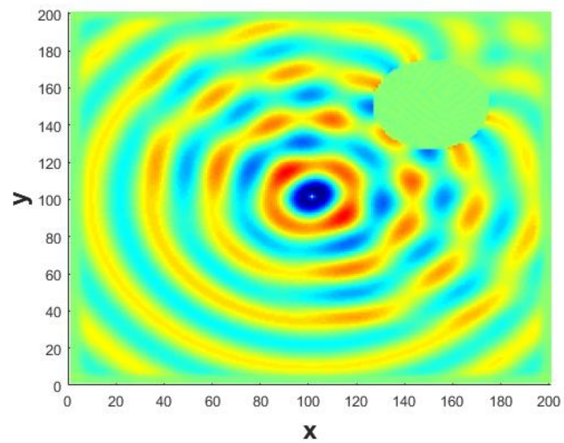

Figure 2.6: Two dimensional wave interaction with dispersive disk

direction . $\triangle t = 0.5\dfrac{\triangle x}{c}$, $x = 300\mu m$, and the number of time steps is 6000. Figure 2.6 is the two dimensional case with a PML boundary . $\lambda = 0.005$, $\omega = \dfrac{2\pi c}{\lambda}$, $\gamma = 4 \times 10^9$, $\omega_p = \dfrac{\omega}{0.29}$, $\triangle x = \triangle y = 0.002$, and the simulation is ran for 1500 time steps.

Chapter 3

TRANSFORMATION OPTICS BASED FDTD ALGORITHM

3.1 Introduction

The Finite-Difference Time-Domain (FDTD) method [1, 2] is a very efficient and effective method for numerically solving Maxwell's equations due to its simplicity, stability, and ability to easily couple a large variety of the material models. As stated earlier, at times this method can become quite expensive computational wise when resolving small and curved structures present in a large computational domain. Many different methods have been developed to improve the efficiency of the FDTD algorithm. One way is to use small grid cells locally near the small object while using large grid cells elsewhere, and this sub-gridding method is reffered [17]. In the past there has been a lot of other sub-gridding and adaptive mesh refinement algorithms developed to solve Maxwell's equations, but a lot of them suffer from late time instabilities and reduced accuracy when the ratio of a space is too large. When small structures are present inside of a large computational domain researchers often use small grid cells locally inside small regions and large grid cells everywhere else. In this work we apply the fully anisotropic FDTD method together with a coordinate transformation (Transformation Optics) to solve Maxwell's equations in complex media. The coordinate transformation we employ maintains the invariance of the Maxwell's equations, but transforms the material into an anisotropic one [11, 12]. In [5] we use the coordinate transformation to achieve local mesh refinement instead of subgridding. We can transform an annulus with a smaller inner radius to an annulus with a larger radius. Since the area of the inner circular region is enlarged, it can be resolved using large grid cells. The trade off is that the annulus region is slightly less resolved because its area becomes smaller. We must make sure that there are enough grid points inside the small region to resolve the wave, therefore the TO based method has some limitations because of the fact that the smaller region cannot be made arbitrarily small. However; the annulus can be controlled to guarantee we have acceptable accuracy. This improves the computational efficiency dramatically if the small region occupies only a tiny portion of the whole computational domain. After this transformation we obtain a new set of anisotrpoic Maxwell's equations which we can solve numerically in another computational space. Since the Maxwell's equations are invariant to this transformation the key properties of the Maxwell's equations still hold after the transformation for the FDTD method such as divergence free, dissipationless, and stability are preserved. In this dissertation, we extend the TO based method to a more general transformation with application to modeling the interaction between optical radiation and subwavelength objects. We show that using transformation optics, we can model the significant enhancement of the scattering cross section of a particle which is referred to as superscattering [13]. In [13] multiple layers of plasmonic materials are added to a dielectric nanorod to design a superscatterer. The plasmonic material is described by the Drude model.

3.2 Transformation Optics Based Maxwell Solver

There are three key steps to the transformation optics based Maxwell solver.

- First we apply a coordinate transformation using transformation optics. Once the transformation is done we obtain a new set of Maxwell's equations with anisotropic permittivity and permeability in the new computational domain.

- Next we solve the new transformed Maxwell's equations in the new computational domain using an anisotropic FDTD algorithm [15, 16].

- Finally once the solution is obtained in the new computational domain it is then transformed back into its original coordinate system to obtain the solution of the original problem.

Now consider the following time dependent Maxwell's equations in Cartesian coordinates (x, y, z)

$$\frac{\partial \vec{D}}{\partial t} = \bigtriangledown \times \vec{H}, \tag{3.1}$$

$$\frac{\partial \vec{B}}{\partial t} = - \bigtriangledown \times \vec{E}, \tag{3.2}$$

$$\vec{D} = \epsilon_0 \epsilon \vec{E}, \tag{3.3}$$

$$\vec{B} = \mu \vec{H}. \tag{3.4}$$

Applying the coordinate transformation from (x, y, z) to (x', y', z'), we obtain a new set in the invariant form of Maxwell's equations.

$$\frac{\partial \vec{D'}}{\partial t} = \bigtriangledown' \times \vec{H'}, \tag{3.5}$$

$$\frac{\partial \vec{B'}}{\partial t} = - \bigtriangledown' \times \vec{E'}, \tag{3.6}$$

where

$$\vec{D'} = \epsilon_0 \epsilon' \vec{E'}, \tag{3.7}$$

$$\vec{B'} = \mu' \vec{H'}. \tag{3.8}$$

In the new coordinates, EM fields and material parameters (permittivity and permeability) are anisotropic, so ϵ' and μ' are tensors. We have,

$$\vec{E'} = \Lambda^T \vec{E'}, \tag{3.9}$$

$$\vec{H'} = \Lambda^T \vec{H'}, \tag{3.10}$$

$$\epsilon' = |\Lambda|\Lambda^{-1}\epsilon\Lambda^{-T}, \tag{3.11}$$

$$\mu' = |\Lambda|\Lambda^{-1}\mu\Lambda^{-T}, \tag{3.12}$$

where Λ is the Jacobian matrix.

$$\Lambda = \begin{pmatrix} X_{x'} & X_{y'} & X_{z'} \\ Y_{x'} & Y_{y'} & Y_{z'} \\ Z_{x'} & Z_{y'} & Z_{z'} \end{pmatrix}, \tag{3.13}$$

and Λ^T represents the transpose of the matrix Λ. To obtain the Jacobian matrix for coordinate scaling we first transform the coordinates from the Cartesian grid to cylindrical coordinates where we get the following

$$\begin{cases} x = r\cos\theta, \\ y = r\sin\theta, \\ z = z. \end{cases} \tag{3.14}$$

Thus we get the following Jacobian matrix

$$\Lambda_1 = \frac{\partial(x,y,z)}{\partial(r,\theta,z)} = \begin{pmatrix} \cos\theta & -r\sin\theta & 0 \\ \sin\theta & r\cos\theta & 0 \\ 0 & 0 & 1 \end{pmatrix}. \tag{3.15}$$

Next we apply a coordinate transform from (r, θ, z) to (r', θ', z') which gives us

$$\begin{cases} r = f(r'), \\ \theta = \theta', \\ z = z'. \end{cases} \tag{3.16}$$

and we get the following Jacobian matrix

$$\Lambda_2 = \frac{\partial(r, \theta, z)}{\partial(r', \theta', z')} = \begin{pmatrix} f'(r') & 0 & 0 \\ 0 & 1 & 0 \\ 0 & 0 & 1 \end{pmatrix}. \tag{3.17}$$

To transform the annulus $R_1 < r < R_2$ to another annulus $R_1' < r' < R_2$ and enlarge the disk $r < R_1$ to $r' < R_1'$, we use the following transformation function

$$r = f(r') = \begin{cases} \dfrac{R_1 r'}{R_1'}, & if \quad r' < R_1' \\ \dfrac{R_1 - R_2}{R_1' - R_2}(r' - R_1') + R_1, & if \quad R_1' \leqslant r' \leqslant R_2 \\ r', & otherwise \end{cases} \tag{3.18}$$

Function f is continuous but not differentiable at $r' = R_1'$ and $r' = R_2'$ as shown in Figure 3.1. We can improve the smoothness of f by using a spline function as shown in Figure 3.2. We can construct a spline function which has continuous derivatives everywhere. In Figure 3.2 we use the following linear polynomial function for the region $x_0 < x < x_1$,

$$S_1(x) = \frac{y_1 - x_0}{x_1 - x_0}(x - x_0) + x_0, \tag{3.19}$$

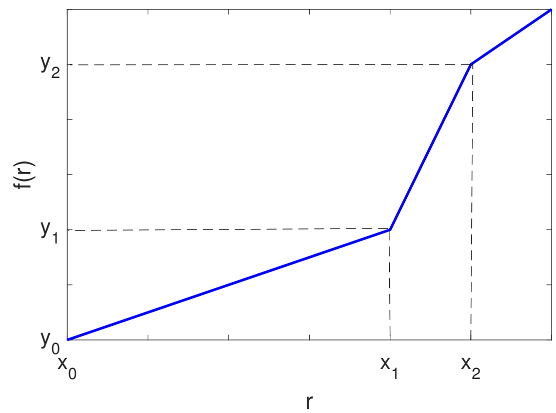

Figure 3.1: Linear spline function

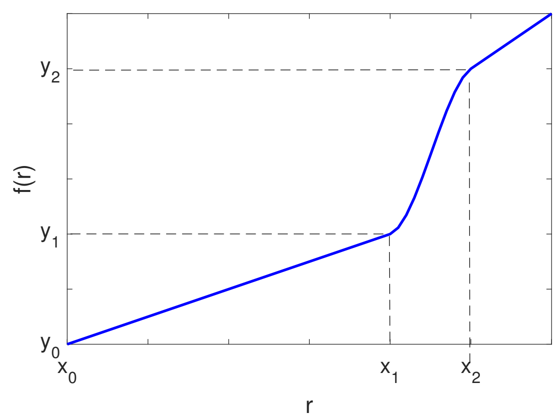

Figure 3.2: Linear and cubic polynomial spline function

and for the region $x_1 < x < x_2$ we use the following cubic polynomial function in

$$S_2(x) = a_3(x - x_2)^3 + a_2(x - x_2)^2 + a_1(x - x_2) + x_2, \tag{3.20}$$

where a_1, a_2, a_3 are computed to guarantee the continuity of the two polynomial functions and the continuity of the derivative of them. Also at $x = x_2$, the slope of $S_2(x) = 1$

Now we transform from cylindrical coordinates (r', θ', z') to Cartesian grid (x', y', z') and we obtain the following,

$$\begin{cases} x' = r' \cos \theta', \\ y' = r' \sin \theta', \\ z' = z', \end{cases} \tag{3.21}$$

hence we get the following Jacobian matrix

$$\Lambda_3 = \frac{\partial(r', \theta', z')}{\partial(x', y', z')} = \begin{pmatrix} \cos\theta' & \sin\theta' & 0 \\ -\frac{\sin\theta'}{r'} & \frac{\cos\theta'}{r'} & 0 \\ 0 & 0 & 1 \end{pmatrix}. \tag{3.22}$$

Combining the three transformations, we get the following

$$\Lambda = \frac{\partial(x, y, z)}{\partial(x', y', z')} = \Lambda_1 \Lambda_2 \Lambda_3 = \begin{pmatrix} \cos\theta & -r\sin\theta & 0 \\ \sin\theta & r\cos\theta & 0 \\ 0 & 0 & 1 \end{pmatrix} \begin{pmatrix} f'(r') & 0 & 0 \\ 0 & 1 & 0 \\ 0 & 0 & 1 \end{pmatrix} \begin{pmatrix} \cos\theta' & \sin\theta' & 0 \\ -\frac{\sin\theta'}{r'} & \frac{\cos\theta'}{r'} & 0 \\ 0 & 0 & 1 \end{pmatrix}. \tag{3.23}$$

Plugging (3.23) into (3.11) and (3.12) we get the material parameters ϵ' and μ'. Yielding this result we can solve the new transformed Maxwell's equations in the new coordinate system (x', y', z') and get the solutions for $\vec{E}$ and $\vec{H}$.

3.3 Dispersive Material

The TO method can be extended to dispersive material also. In chapter 2 we have the relative permittivity ϵ for Drude material

$$\epsilon = \epsilon_\infty - \frac{\omega_p^2}{\omega^2 - j\gamma\omega}, \tag{3.24}$$

where ω_p is the plasma frequency, ω is the incident frequency, ϵ_∞ is the permittivity of free space, and γ is the damping or loss term. Plugging (3.24) into (3.7) we get the following.

$$\vec{D'} = \epsilon_0 \epsilon' \vec{E'}, \tag{3.25}$$

$$\vec{D'} = \epsilon_0 |\Lambda| \Lambda^{-1} \epsilon \Lambda^{-T} \vec{E'}, \tag{3.26}$$

$$\vec{D'} = \epsilon_0 |\Lambda| \Lambda^{-1} \left(\epsilon_\infty - \frac{\omega_p^2}{\omega^2 - j\gamma\omega} \right) \Lambda^{-T} \vec{E'}, \tag{3.27}$$

$$\vec{D'} = \epsilon_0 |\Lambda| \Lambda^{-1} \epsilon_\infty \Lambda^{-T} \left(1 - \frac{\frac{\omega_p^2}{\epsilon_\infty}}{\omega^2 - i\gamma\omega} \right) \vec{E'}. \tag{3.28}$$

Let

$$\hat{P} = -\frac{\frac{\omega_p^2}{\epsilon_\infty}}{\omega^2 - i\gamma\omega} \vec{E'}, \tag{3.29}$$

and

$$\tilde{\epsilon} = \epsilon_0 |\Lambda| \Lambda^{-1} \epsilon_\infty \Lambda^{-T}, \tag{3.30}$$

we get the following constitutive equation

$$\vec{D'} = \tilde{\epsilon}(\vec{E'} + \vec{P}). \tag{3.31}$$

Recall the Auxiliary Differential Equation we used in chapter two to derive the differential equation for the conduction current term J. Here we can perform the same algorithm for the polarization vector $\hat{P}$ and we get

$$\vec{P}\left(\omega^2 - i\gamma\omega\right) = -\frac{\omega_p^2}{\epsilon_\infty} \vec{E'}, \tag{3.32}$$

$$\vec{P}\omega^2 - i\gamma\omega\vec{P} = -\frac{\omega_p^2}{\epsilon_\infty} \vec{E'}. \tag{3.33}$$

Taking the inverse fourier transform of (3.33) we get the following differential equation

$$\frac{\partial^2 \vec{P}}{\partial t^2} + \gamma \frac{\partial \vec{P}}{\partial t} = \frac{\omega_p^2}{\epsilon_\infty} \vec{E}'. \tag{3.34}$$

Thus we use equation (3.31) to update the electric field $\vec{E}$

$$\vec{E} = \tilde{\epsilon}^{-1} \vec{D} - \vec{P}. \tag{3.35}$$

3.3.1 Coordinate Scaling

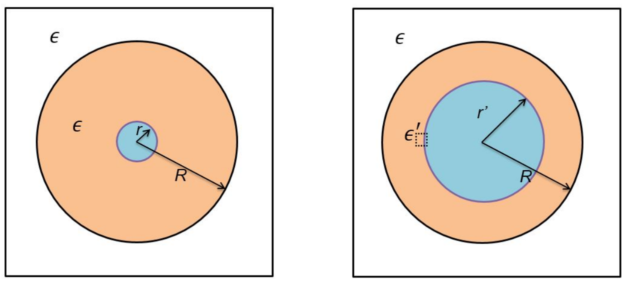

Figure 3.3: Coordinate scaling in radial direction. Left: the physical domain; Right: the computational domain.

As shown in Fig 3.3, the circular region with radius R is modified by enlarging an inner disk with radius r to r'. By this coordinate scaling, the small disk in the physical domain becomes a larger one in the computational domain. The FDTD Maxwell solver is applied in the computational domain with the Cartesian grid, so that the disk with radius r' has more grid points in it than it is in the physical domain. It has a magnifier effect and we will be able to see more clear in this particular region with radius r'. A trade off is that the annulus (r, R) is shrunk to a thinner annulus (r, R). Usually this method applies to the case where the structure is subwavelength, so that the wave is still resolved in the thinner annulus after the coordinate scaling. This mapping can be used inversely to make a thin layer annulus thicker.

3.3.2 Coordinate Rotation

In the section, we show how to apply the TO technique to rotate the mesh so that the staircase approximation for an oblique object can be eliminated. Similar to the previous section, the coordinate rotation is done in polar coordinates. We first transform the domain from Cartesian coordinates to polar coordinates, then the coordinate rotation is done through a mapping function about the angle,

$$\theta = f(\theta') = \theta' + \alpha(r).$$

Finally it is transformed back to Cartesian grid. Here in order to have a smooth mapping with continuous derivatives, we let the rotation angle be a function $\alpha(r)$ of the radius r from the location to the center of the rotation. Fig. 3.4 shows the coordinate rotation and the corresponding mesh in the original physical domain and the transformed Cartesian mesh in computational domain. Through the coordinate rotation we see that the staircase approximation caused by the tilted square can be eliminated. Details on the simulation results are shown in Chapter 4.

3.3.3 Coordinate Translation

Besides the coordinate scaling and rotation, we can also apply translation. For example, for the case when we simulate two objects with a very small gap, instead of using scaling, we can use translation to separate the two objects further so that the gap region can be modeled with more grid points. Different from the previous two cases where the coordinate changes are done in polar coordinates, the coordinate translation is performed in Cartesian mesh. No Cartesian to polar and polar to Cartesian transformation is needed. Fig. 3.5 shows the coordinate translation and the corresponding mesh in the original physical domain and the transformed Cartesian mesh in computational domain. Through the

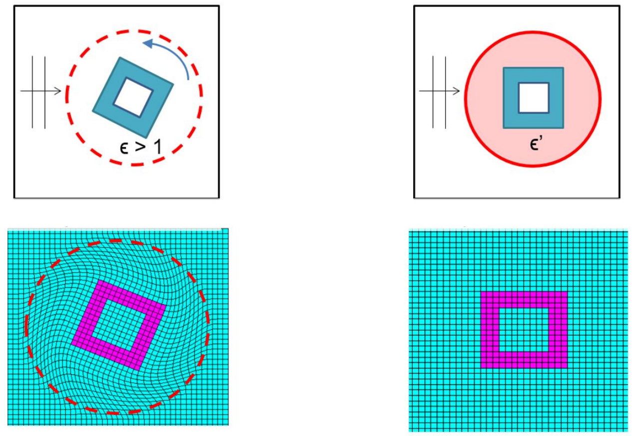

Figure 3.4: Coordinate rotation. Left: physical domain. Right: computational domain. Upper row: the geometry. Lower left: the non-Cartesian mesh in the physical domain; Lower right: the transformed Cartesian mesh in the computational domain.

coordinate translation the gap region has finer grid so the gap is virtually larger in the computational domain. With more grid points in the gap region we obtain more accurate solution. Numerical examples will be presented in chapter 4.

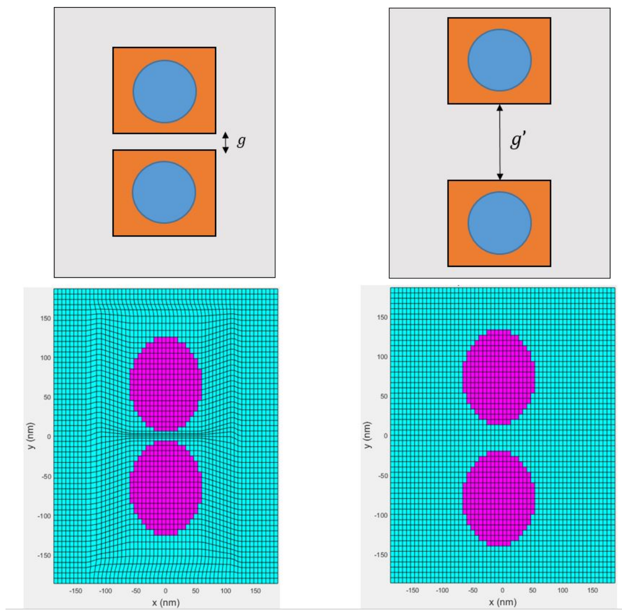

Figure 3.5: Coordinate translation. Left: physical domain. Right: computational domain. Upper row: the geometry. Lower left: the non-Cartesian mesh in the physical domain; Lower right: the transformed Cartesian mesh in the computational domain.

Chapter 4

NUMERICAL SIMULATIONS

In this chapter, we show some numerical examples using the proposed TO-FDTD method.

4.1 Scattering simulation of a dielectric cylindrical shell

We start with the two dimensional scattering problem of a dielectric cylindrical shell. Each cylinder is placed at the center of the computational domain. We choose our computational domain to be 5 $\mu m \times 5$ μm. We also use a uniform Cartesian mesh grid size $\triangle x = \triangle y$, denoted by $\triangle$. The incident wave is a plane wave polarized in the $y-$ direction (TEz) and propagates in the $x-$ direction. The wavelength of the incident plane wave is 1.2 μm. The inner radius of the cylinder is $R_1 = 1500$ nm and the outer radius of the cylinder is $R_2 = 1600$ nm. The dielectric constant of the cylindrical shell is 9. Transformation optics is applied to transform the annulus to a thicker annulus. The inner radius of the cylinder is shrunk to $R_1' = 1400$ nm, so the thickness of the layer is doubled. In this result we notice that the TO method gives a similar level of accuracy that the standard FDTD method does with half the grid size.

Figure 4.1 shows the cylinder with a larger inner radius being shrunk to a smaller radius and the corresponding meshes in physical and computational domains. Figure 4.2 shows the electric field distribution near the cylindrical shell. The comparison between standard FDTD with different mesh size and the TO-FDTD shows that the TO-FDTD method with 100×100 mesh has similar results as the FDTD with doubled mesh size 200×200.

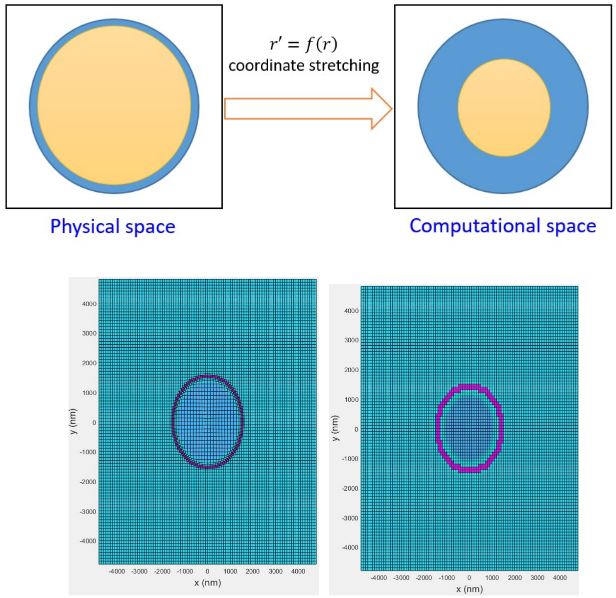

Figure 4.1: Coordinate scaling to enlarge the thickness of a thin layer cylindrical shell. Left: the physical space. Right: the computational space. Upper row: the geometry of the transformation. Lower row: the meshes.

4.2 Scattering simulation of a tilted square

In this section, we apply a coordinate rotation to the case where the scatter is a tilted square. Figure 4.3 shows the coordinate rotation using the TO method and the corresponding meshes in the physical and computational domain. Figure 4.4 shows the comparison of the standard FDTD with the TO method. The standard FDTD has the staircase error near the material interface while the TO method is smoother. First row of Fig. 4.4 shows the staircased FDTD mesh together with the solution with physical spikes near the material interface. In contrast the TO mesh does not have staircase and the solution is smooth near the material interface.

4.3 Simulation of two metal disks with small gap

In this section, we simulate two metal disks with radius 60 nm separated with a small gap of 5 nm. We study the field enhancement in the gap region. We apply TO to enlarge the surrounding area of the gap so that this region can be resolved using a large grid size. We plot the field enhancement at a selected location which is the center of gap. The material of the metal disk is modeled using Drude model with $\epsilon_\infty = 1$, $\omega_p = 0.99 \times 10^{16}$ and $\gamma = 2.2 \times 10^{14}$. The computational domain $0.4\ \mu m \times 0.4\ \mu m$. Figure 4.5 shows the geometry of the simulation and the meshes in the physical and computational domain. Figure 4.6 shows the simulation results and comparison between FDTD and TO-FDTD. The TO-FDTD with low 100×100 mesh ha similar spectrum as the FDTD with doubled mesh 200×200.

4.4 Superscattering Simulations

In this section, we simulate the superscattering proposed in [13]. The superscatter is a metal particle coated with one layer of dielectric material and then the second layer with metal, so it is a particle of metal-dielectric-metal layered material. The planewave propagates in x-direction with wavelength 1 μm which corresponds to angular frequency $\omega = 1885\ THz$. The dielectric constant is $\epsilon = 12.96$. The metallic material is modeled using Drude model with $\epsilon_\infty = 1$, $\omega_p = \omega/0.2542$, and $\gamma = 0$. The radius of the three layers are: $r_1 = 0.3485\lambda_p$, $r_2 = 0.5623\lambda_p$, and $r_3 = 0.6370\lambda_p$, where $\lambda_p = \dfrac{2\pi c}{\omega_p}$ with c being the speed of light. The computational domain is $12\ \mu m \times 12\ \mu m$. The mesh sizes are 300×300 and 600×600, and 1200×1200. The simulation setup is shown in Fig 4.7. We apply coordinate scaling to enlarge the particle by a factor of 4.

The simulation results of poynting vector S_x distributions are shown in Fig 4.8. Also for the standard FDTD method with a mesh of 1200×1200 when ran for 3000 time steps the CPU time is 1034 seconds, where as for the TO method with a mesh of 300×300 when it is ran out for 3000 time steps the CPU time is only 34 seconds. The regular particle (non-superscatter) result is shown in Fig. 4.8(a). Fig. 4.8 (b)-(d) show the results of FDTD with 300×300, 600×600, and 1200×1200, respectively. The higher resolution, the

Table 4.1: Time Comparison Table

(a) FDTD 300×300	(b) FDTD 600×600	(c) FDTD 1200×1200	(d) TO-FDTD 300×300
16 seconds	135 seconds	1,034 seconds	34 seconds

stronger the superscattering effect is by looking at the shade behind the particle. Fig. 4.8 (e) and (f) show the TO-FDTD results with 300×300 and 600×600 meshes. We can see that the TO-FDTD with smaller mesh has a comparable result with FDTD of a larger mesh, while the TO method takes less CPU time, so the TO method is more efficient than the FDTD.

Table 4.1 shows a comparison between the standard FDTD method of grid meshes $300 \times 300, 600 \times 600$, and 1200×1200, and the TO-FDTD with grid mesh 300×300. In this table we see that the TO-FDTD method significantly improves the efficiency of the standard FDTD method.

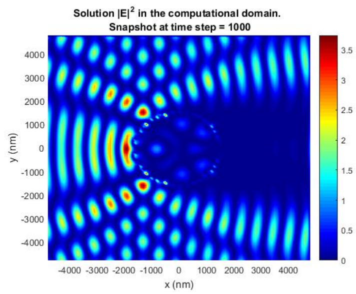

(a)

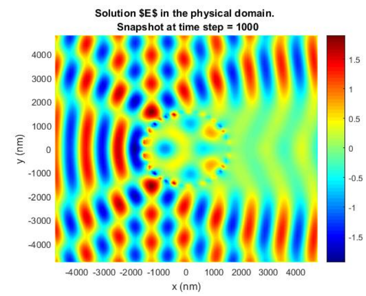

(b)

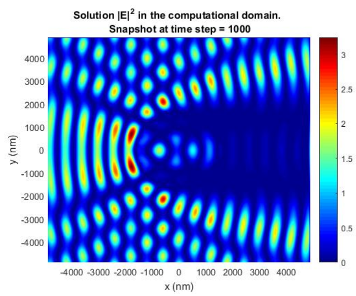

(c)

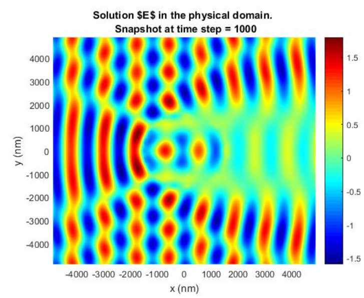

(d)

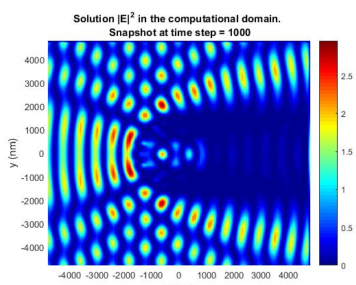

(e)

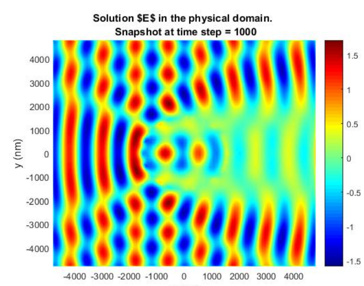

(f)

Figure 4.2: Simulation results of scattering from a cylindrical shell. Left column: Electric intensity distribution. Right column: Electric field distribution. First row: FDTD results with 100×100 mesh. Second row: FDTD results with 200×200 mesh. Third row: TO-FDTD results with 100×100 mesh.

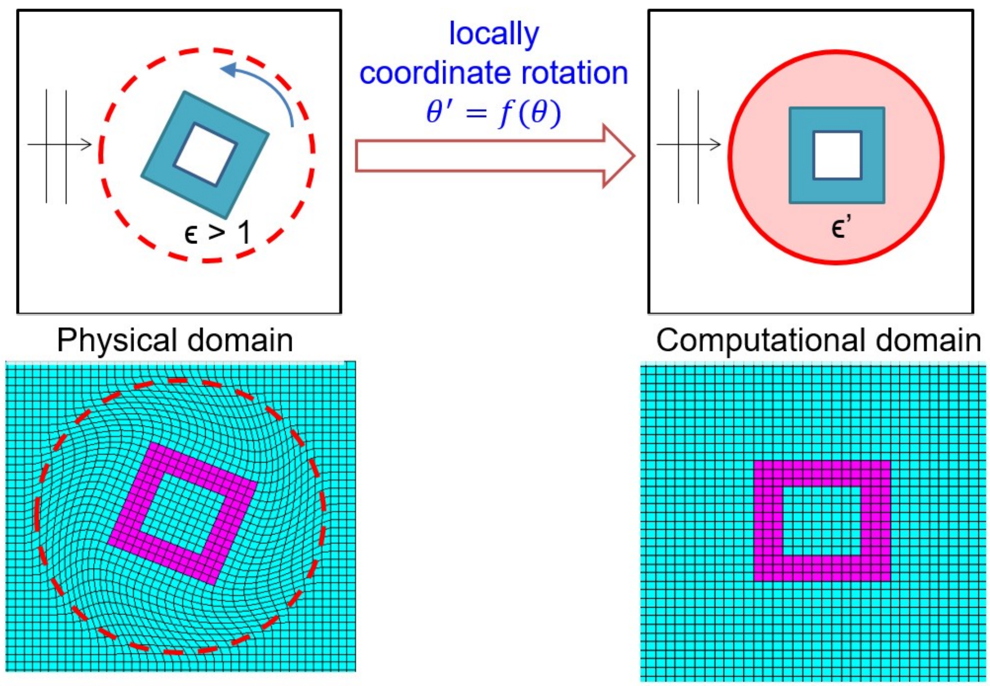

Figure 4.3: A locally coordinate rotation and the corresponding meshes in the physical (lower left) and computational (lower right) domains.

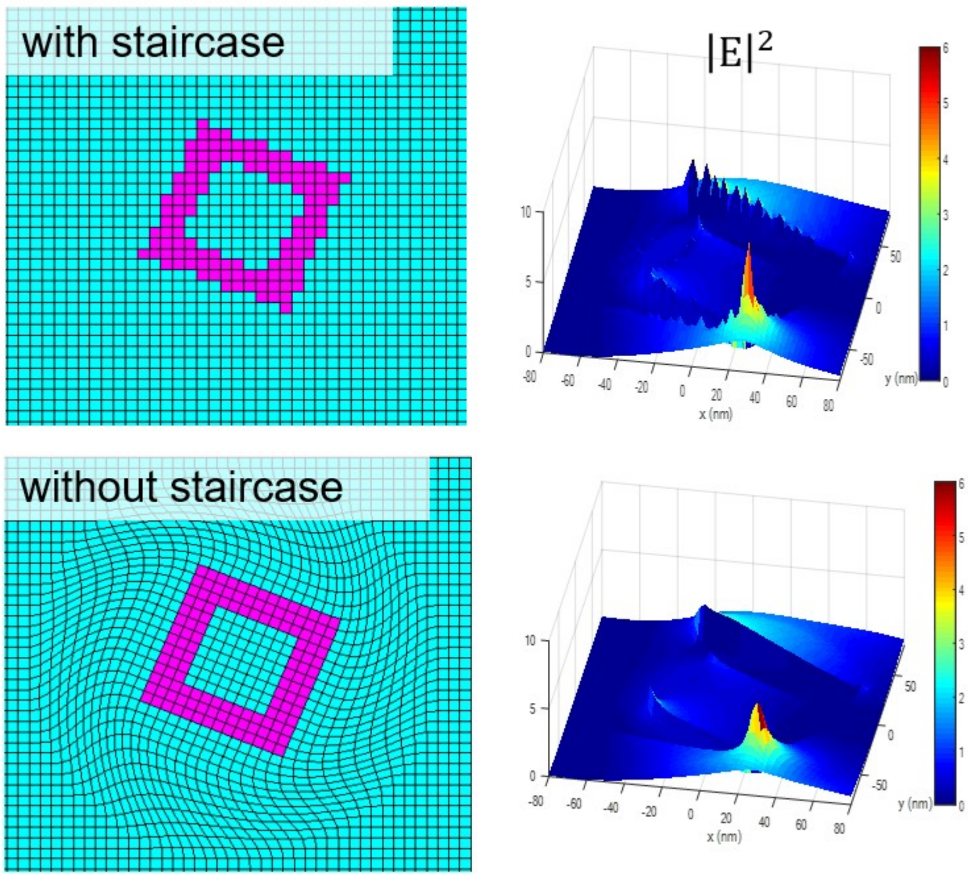

Figure 4.4: Scattering simulation of a titled square. Upper row: FDTD result with staircase effect. Lower row: TO-FDTD result without the staircase effect. Left column: the meshes; Right column: the surface plot of the field intensity $|E^2|$.

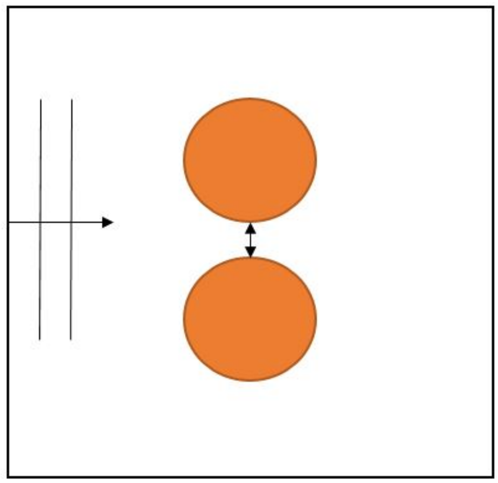

(a)

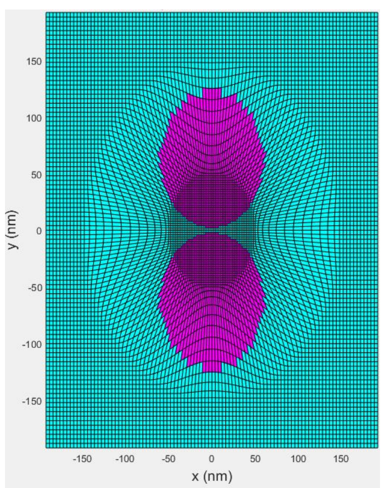

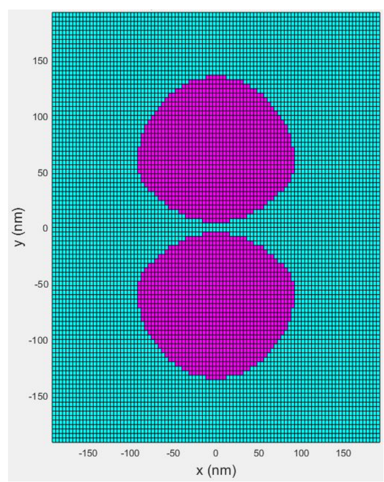

(b) (c)

Figure 4.5: (a) The geometry of the simulation, (b) the meshes in the physical domain and (c) in the computational domain .

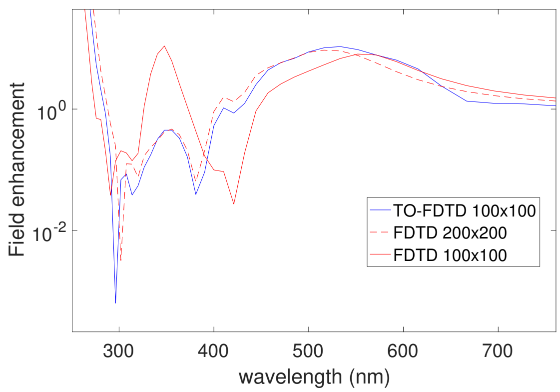

Figure 4.6: Field enhancement in the center of the two metal disks and comparison between FDTD with different resolution and the TO-FDTD method.

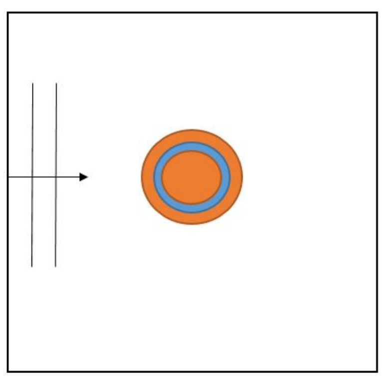

Figure 4.7: The simulation setup of the superscattering simulation.

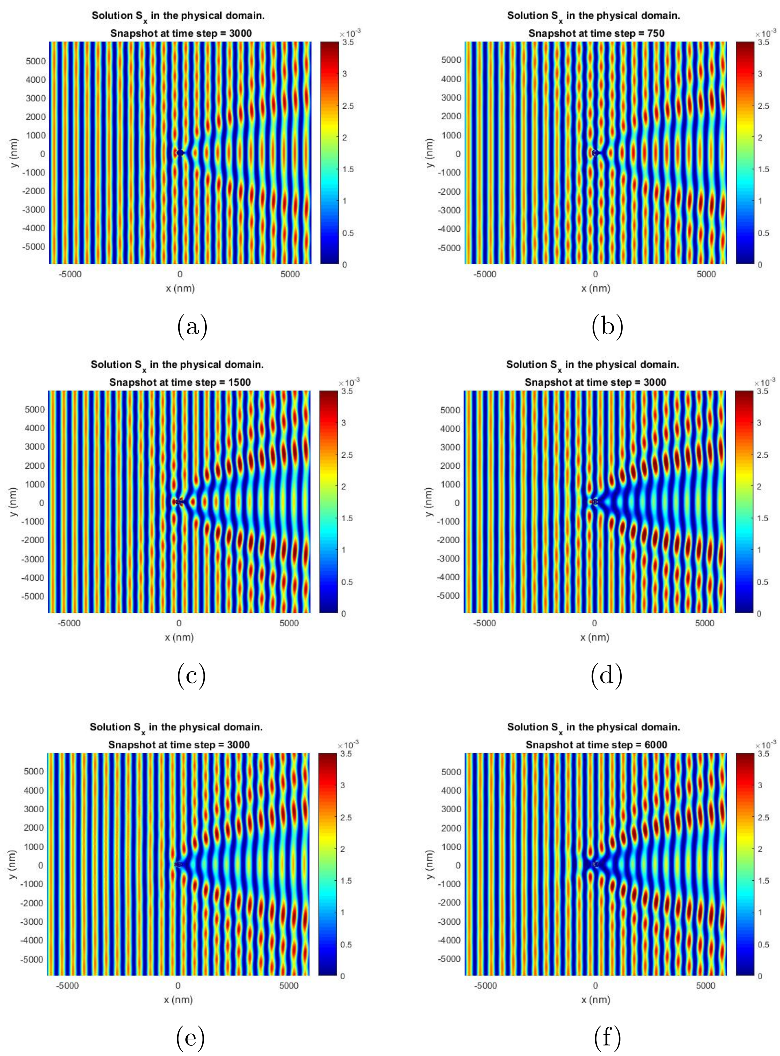

Figure 4.8: Simulation results of the Poynting vector S_x distribution. (a) The regular non-superscatterer. The FDTD results of superscatter with meshes (b) 300×300; (c) 600×600; (d) 1200×1200. The TO results of superscatter with meshes (e) 300×300 and (f) 600×600

Chapter 5

CONCLUSION

In conclusion, we have studied the transformation optics-based FDTD method for solving Maxwell's equations. We have shown how applying a coordinate transformation can be employed to map an irregular mesh to a cartesian mesh. We have studied the anisotropic FDTD algorithm that solves the transformed Maxwell's equations in the new transformed grid, how coordinate scaling eliminates multiple sub-gridding, how a coordinate rotation can eliminate the staircase effect, and how a translation transformation can also enlarge a certain region of interest. These transformations allow us to obtain more efficiency. The modeling of the scattering and superscattering simulations validates our claim for this analysis. We have shown that the TO method can achieve the same level of accuracy or more with half the grid size mesh compared to the standard FDTD method. The time comparison table shows that the computational cost is reduced significantly compared to that of the standard FDTD method. This validates our claim for efficiency. We were able to model dispersive materials with application to superscattering. In the future we plan to look at modeling nonlinear dispersive materials, superscatterers in a three dimensional space, and model a graphene based superscatterer.

The challenge for modeling nonlinear dispersive materials would be the update of nonlinear constitutive equations with the anisotropic FDTD algorithm. Also, in the future, we would like to look into modeling a graphene coated nano-cylinder illuminated by a electromagnetic plane wave in the far-infrared range of frequencies. The most challenging part will be trying to obtain the resonance effect that graphene gives with a certain frequency. This will enable more applications to this research.

REFERENCES

[1] Allen Taflove and Susan C Hagness. Computational electrodynamics: the finite-difference time-domain method. *Artech house, 2005.*

[2] Kane Yee. Numerical solution of initial boundary value problems involving maxwells equations in isotropic media. IEEE Transactions on antennas and propagation, 14(3):302–307, 1966.

[3] Sarker, Pejush Chandra and Rana, Md Masud and Sarkar, Ajay Krishno A simple FDTD approach for the analysis and design of graphene based optical devices Optik-International Journal for Light and Electron Optics , 144, 1–8, 2017, Elsevier

[4] Xu, Ning and Chen, Juan and Wang, Jianguo and Qin, Xijia and Shi, Jiepei Dispersion HIE-FDTD method for simulating graphene-based absorber

IET Microwaves, Antennas & Propagation, 11, 1, 92–97, 2017, IET

[5] Jinjie Liu, Moysey Brio, and Jerome V Moloney. Transformation optics based local mesh refinement for solving maxwells equations. Journal of Computational Physics, 258:359–370, 2014.

[6] Huidobro, Paloma A and Kraft, Matthias and Kun, Ren and Maier, Stefan A and Pendry, John B Graphene, plasmons and transformation optics

Journal of Optics, 18, 4, 044024, 2016, IOP Publishing

[7] Wang, Huaping and Deng, Yangyang and Zheng, Bin and Li, Rujiang and Jiang, Yuyu and Dehdashti, Shahram and Xu, Zhiwei and Chen, Hongsheng Panoramic lens designed with transformation optics Scientific reports, 7, 40083, 2017, Nature Publishing Group

[8] Jiang, Jing and Zhang, Daohua and Zhang, Baile and Luo, Yu Interaction between graphene-coated nanowires revisited with transformation optics Optics letters,42,15,2890–2893,2017,Optical Society of America

[9] Qian, Chao and Lin, Xiao and Yang, Yi and Gao, Fei and Shen, Yichen and Lopez, Josue and Kaminer, Ido and Zhang, Baile and Li, Erping and Soljacic, Marin and others Multifrequency superscattering from subwavelength hyperbolic structures ACS Photonics, 5, 4, 1506–1511, 2018, ACS Publications

[10] Salski, Bartlomiej An FDTD model of graphene intraband conductivity IEEE Transactions on Microwave Theory and Techniques, 62, 8, 1570–1578, 2014,

[11] *John B Pendry, David Schurig, and David R Smith. Controlling electromagnetic fields. Science, 312(5781):1780–1782, 2006.*

[12] *Ulf Leonhardt. Optical conformal mapping. Science, 312(5781):1777–1780, 2006.*

[13] *Ruan, Zhichao and Fan, Shanhui Superscattering of light from subwavelength nanostructures Physical review letters 105,1,013901,2010, APS*

[14] *Li, RJ and Lin, X and Lin, SS and Liu, X and Chen, HS Tunable deep-subwavelength superscattering using graphene monolayers Optics letters, 40, 8, 1651–1654, 2015, Optical Society of America*

[15] *Werner, Gregory R and Cary, John R A stable FDTD algorithm for non-diagonal, anisotropic dielectrics Journal of Computational Physics,226,1,1085–1101,2007,Elsevier*

[16] *Werner, Gregory R and Bauer, Carl A and Cary, John R A more accurate, stable, FDTD algorithm for electromagnetics in anisotropic dielectrics Journal of Computational Physics ,255,436–455,2013,Elsevier*

[17] *Jean-Pierre Bérenger. The huygens subgridding for the numerical solution of the maxwell equations. Journal of Computational Physics, 230(14):5635–5659, 2011.*

[18] *Vakil, Ashkan and Engheta, Nader Transformation optics using graphene Science, 332, 6035, 1291–1294, 2011, American Association for the Advancement of*

[19] *Li, Rujiang and Zheng, Bin and Lin, Xiao and Hao, Ran and Lin, Shisheng and Yin, Wenyan and Li, Erping and Chen, Hongsheng Design of ultracompact graphene-based superscatterers IEEE Journal of Selected Topics in Quantum Electronics, 23, 1, 130–137, 2017,*

[20] *Naserpour, Mahin and Zapata-Rodriguez, Carlos J and Vukovic, Slobodan M and Pashaeiadl, Hamid and Belic, Milivoj R Tunable invisibility cloaking by using isolated graphene-coated nanowires and dimers Scientific reports, 7, 1, 12186, 2017, Nature Publishing Group*

[21] *Ruan, Zhichao and Fan, Shanhui Design of subwavelength superscattering nanospheres Applied Physics Letters, 98, 4, 043101, 2011, AIP*

[22] *Schneider, John B Understanding the finite-difference time-domain method School of electrical engineering and computer science Washington State University.–URL: http://www. Eecs. Wsu. Edu/˜ schneidj/ufdtd/(request data: 29.11. 2012), 2010*